TECHNICAL MEMORANDUM

ANL-CT-81-42

TUBE VIBRATION IN INDUSTRIAL-SIZE TEST HEAT EXCHANGER (30° TRIANGULAR LAYOUT - SIX-CROSSPASS CONFIGURATION)

by

M. W. Wambsganss, H. Halle,
and W. P. Lawrence

ARGONNE
NATIONAL
LABORATORY

Prepared for
U. S. DEPARTMENT OF ENERGY
under Contract W-31-109-Eng-38

DISCLAIMER

Printed in the United States of America
Available from
National Technical Information Service
U. S. Department of Commerce
5285 Port Royal Road
Springfield, VA 22161

NTIS price codes
Printed copy: A05
Microfiche copy: A01

TECHNICAL MEMORANDUM

ANL-CT-81-42

Distribution Category:
Energy Conservation—
Industry (UC-95f)

ANL-CT--81-42

DE82 008578

ARGONNE NATIONAL LABORATORY
9700 South Cass Avenue
Argonne, Illinois 60439

TUBE VIBRATION IN INDUSTRIAL-SIZE TEST HEAT EXCHANGER (30° TRIANGULAR LAYOUT - SIX-CROSSPASS CONFIGURATION)

by

M. W. Wambsganss, H. Halle,
and W. P. Lawrence

Components Technology Division

October 1981

THIS PAGE

WAS INTENTIONALLY

LEFT BLANK

TABLE OF CONTENTS

NOMENCLATURE

C_f ≡ Instability function for fluidelastic-stiffness-controlled instability

C_g ≡ Instability function for fluid-damping-controlled instability

d ≡ Tube diameter

f ≡ Natural frequency

m ≡ Mass per unit length of tube

P ≡ Tube pitch

Q ≡ Shellside flowrate

T ≡ Transverse spacing of tube

L ≡ Longitudinal spacing of tube

U ≡ Mean cross flow velocity through minimum gap

ζ ≡ Modal damping ratio

ρ ≡ Fluid density

Δp ≡ Overall (inlet-to-outlet) pressure drop

Superscripts

v ≡ In vacuo (in air) conditions

w ≡ In water conditions

LIST OF FIGURES

LIST OF FIGURES (Contd.)

LIST OF TABLES

ABSTRACT

Tube vibrations in heat exchangers are being systematically studied in a series of tests performed with an industrial-size test exchanger. Results from flow tests of nine different tube bundles, in a basic 5-baffle, 6-crosspass configuration on a 30°-triangular layout with a pitch-to-diameter ratio of 1.25, are reported. The test cases include a full tube bundle, no-tubes-in-window bundle, finned tube bundle, and several proposed field fixes. The testing focused on identification of the lowest critical flowrate to initiate fluidelastic instability (large amplitude tube motion) and the location within the bundle of the tubes which first experience instability. The threshold flowrates are determined from a combination of methods based on sensory observations, vibration amplitude data, and frequency response information. Pressure drop data is also generated and reported.

I. INTRODUCTION

Tube vibrations in heat exchangers are being systematically studied in a series of tests performed with an industrial-size test exchanger. The tests are part of an on-going Heat Exchanger Tube Vibration Program[1] sponsored by the U.S. Department of Energy as an element of the Physical Processes Project within the Energy Conversion and Utilization (ECUT) Program. The Heat Exchanger Tube Vibration Program also includes the development of a data bank of field experiences with tube vibrations, and dissemination and use of the data to develop and validate prediction methods and design guides. It is significant that Heat Transfer Research, Inc. (HTRI), a not-for-profit research organization with over 150 members representing heat exchanger designers, manufacturers, and users, is retained as a consultant to the program. HTRI provides an important link with industry and needed input relative to designs of interest, design fixes, problems experienced, and the like.

Tubes in a heat exchanger will vibrate at virtually all flowrates to which they are exposed. At low flowrates the response is of low amplitude and typically random in character; a number of the closely spaced coupled modes are excited. These vibrations are generally acceptable; however, consideration must be given to the potential for long term wear at the tube/support interfaces. When the shellside flowrate is increased to exceed a threshold value, fluidelastic instability occurs. This is an excitation mechanism responsible for large amplitude vibration which, among other things, can result in tube-to-tube impacting and cause rapid tube failure. As such, it is the mechanism of most concern to designers and is the focus for this testing program.

A test exchanger, representative of a segmentally baffled, industrial-size, shell-and-tube heat exchanger has been designed and fabricated specifically for this test program. The exchanger is shown in Fig. 1 as installed in the Argonne National Laboratory's Flow Induced Vibration Test Facility (FIVTF), and is described in a later section of this report.

Tests with eight-crosspass (seven equally spaced baffles) bundles on a 30° triangular layout with a pitch-to-diameter ratio of 1.25 have been completed and reported.[2] Five different test cases were studied. These include three different inlet/outlet nozzle diameters for both full bundle and no-tubes-in-window (NTIW) configurations. In summary, results from

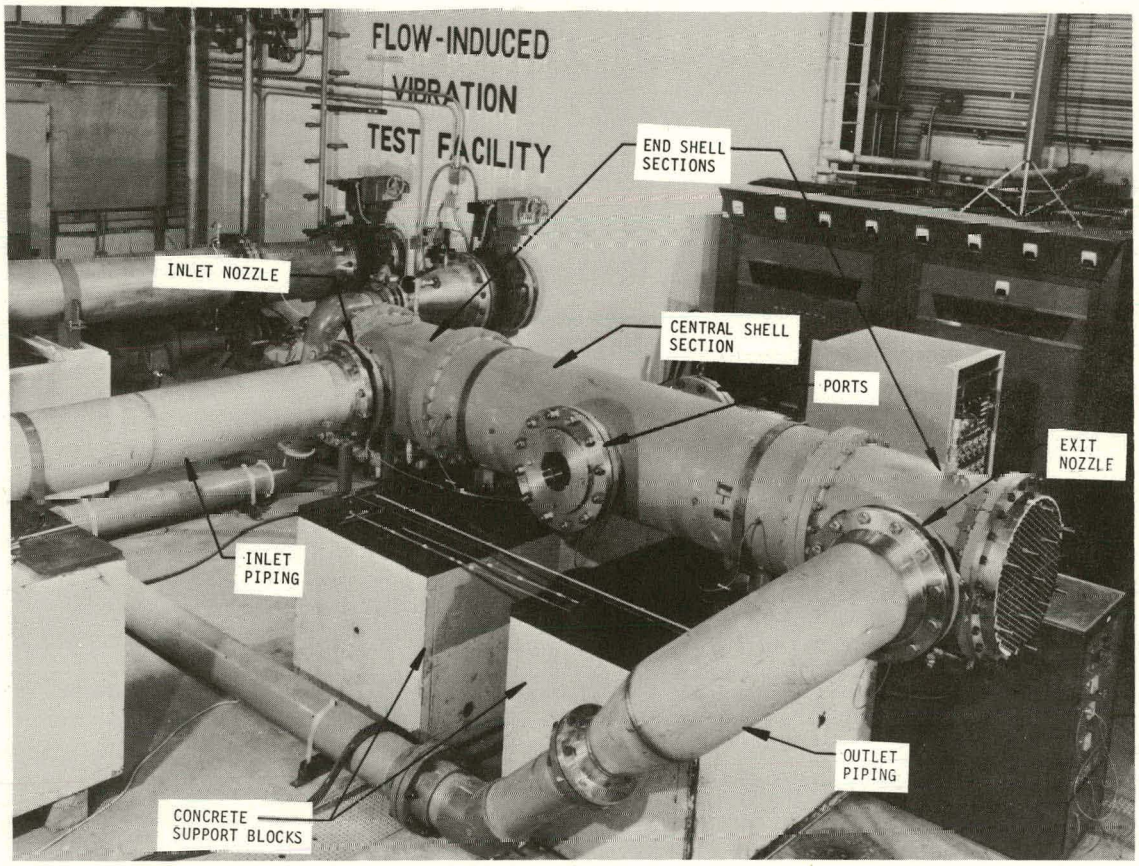

Fig. 1. Test exchanger installed in Flow-Induced Vibration Test Facility (FIVTF)

these tests showed that tubes in the first two rows past the baffle cut in the far window region, opposite the inlet/outlet nozzles, are the first to experience instability. As the flowrate is increased further, adjacent groups of tubes in the far window region participate in the instability. Typically, hysteresis is observed in the sense that the flowrate at which instability ceases is below the threshold value for the onset of instability. Also, for the range of diameters tested, inlet/outlet nozzle size did not have a significant effect on critical flowrate.

This report presents the results of tests with six-crosspass (five equally spaced baffles) bundles, also on a 30° triangular layout with a pitch to diameter ratio of 1.25. Ten different test cases are reported. The test cases include a full tube bundle, NTIW bundle, finned tube bundle, and several proposed field fixes. As in the previous tests with eight-crosspass bundles, the primary objective of the testing is to determine the critical flowrate for fluidelastic instability and to identify the locations within the bundle of the tubes which first experience instability.

II. BACKGROUND

Fluid structure coupling in closely spaced tube bundles and fluidelastic instability phenomena have been the subjects of a considerable number of research studies during the last decade. In particular, several recently published papers[3-5] have contributed to our understanding of fluidelastic instability in tube bundles. These new results are useful in interpreting the subject tests and consequently will be reviewed below along with criteria for determining the critical flow velocity.

A. Instability Mechanisms

In a two-part, benchmark paper,[3,4] Chen uses a previously developed mathematical model to examine the mechanisms responsible for fluidelastic instability and to develop stability criteria. From an analysis of the equations of motion for a group of cylinders, it is found that there are two types of dynamic instability: fluid-damping-controlled instability and fluidelastic-stiffness-controlled instability.

Fluid-damping-controlled instability is caused by the fluid damping force. When the flow velocity exceeds a critical value, the modal damping becomes negative and the system becomes unstable. Tube velocity is the controlling feature and hence the mechanism may be referred to as a "velocity mechanism." The instability mode will be one of the classical modes. An important feature of this type of instability is that fluid damping coupling with other tubes is not a necessary condition. Consequently, a single elastic tube in an otherwise rigid array can experience instability.

Fluidelastic-stiffness-controlled instability is the dynamic instability caused by fluidelastic forces. Tube displacement is controlling in this case and the mechanism is called a "displacement mechanism." the fluidelastic forces contribute to modal damping of the coupled modes and may act to reduce damping. When the modal damping becomes zero the system becomes unstable. In this case, the instability mode is not one of the classical modes; phase difference among the tubes is the essential feature. Fluidelastic coupling between adjacent tubes is a necessary condition and a single elastic tube in a rigid array will not lose stability by this mechanism.

In general, both fluidelastic and fluid damping forces contribute to the dynamic instability. While a closed form solution cannot be obtained

for the general case, the stability criterion can be written in functional form as[3]

$$\frac{U}{fd} = F\left(\frac{m}{\rho d^2}, \zeta, \frac{T}{d}, \frac{L}{d}, \text{turbulence characteristics}\right) . \quad (1)$$

In gas flows the instability is dominated by the displacement mechanism and is fluidelastic-stiffness-controlled. The stability criterion can be written in closed form as[3]

$$\left(\frac{U}{fd}\right) = \frac{\sqrt{2\pi}}{C_f}\left(\frac{2\pi\zeta m}{\rho d^2}\right)^{0.5} . \quad (2)$$

In liquid flows the instability is fluid-damping-controlled and attributed to the velocity mechanism. The stability criterion can be written as[3]

$$\left(\frac{U}{fd}\right) = \frac{4}{C_g}\left(\frac{2\pi\zeta m}{\rho d^2}\right) . \quad (3)$$

In Eqs. (2) and (3) the parameters C_f and C_g are functions of the fluidelastic and fluid damping force coefficients, respectively. In general, C_f and C_g will also be functions of flow velocity.

In Eqs. (1)-(3) the values for modal damping ζ, mass per unit length m, and natural frequency f can be either those determined in vacuo or those determined in still fluid.[4] Chen notes that the in-fluid parameters are typically difficult to determine in liquids because of the fluid structure coupling. He goes on to suggest that in practical situations it may be more convenient to use the in-vacuo parameters. Of course, if the in-vacuo parameters are used the appropriate (in-vacuo) functions for C_f and C_g must also be used.

Yeung and Weaver[5] studied the effect of incident flow direction on the critical flow velocity for a tube bundle on an equilateral triangular layout. They used a specially designed rig that allows the tube bundle to be rotated through a range of angles relative to the incoming flow. Results of the experimental study, performed in water, show that the instability threshold for a 30° (normal) triangular layout is very sensitive to incident flow direction: A change in orientation of 8° can cause a 50% reduction in critical flow velocity. On the other hand, the 60° (parallel) triangular layout is rather insensitive to incident flow direction: the

critical flow velocity increases only slightly for orientations up to 20°. See Fig. 2. The results obtained by Yeung and Weaver agree with those reported by Soper[6] for the extremes of a 30° and 60° triangular layout.

The results from these recent studies of fluidelastic instability in tube bundles have implications in the analysis and interpretation of data from the subject heat exchanger tube vibration tests. The heat exchanger tests are performed with water on the shellside. From Chen's work[3,4] it is concluded that with liquid flow, and a fluid-damping-controlled instability, coupling with neighboring tubes is not a necessary condition for instability and a single flexible tube in a rigid bundle can experience instability. This implies that detuning will not have a significant effect on the critical flowrate. In a real heat exchanger, corresponding natural frequencies of tubes, having identical number of spans, may vary due to differences in intermediate supports, end fixity, and material properties. In light of the above conclusion these variations should not be expected to affect the instability. Additionally, it can be expected that a single tube may go unstable without the coupling of adjacent tubes. That is, it is not necessary that a group or row of tubes experience instability at the same time.

Chen's results,[3,4] together with those of Weaver and Grover,[7] also show that the critical flow velocity is only weakly dependent on damping. As with the natural frequencies, damping can be expected to vary from tube to tube within a real heat exchanger. Again, these variations are not expected to have a significant effect on critical flowrate because of the weak dependence on damping.

In a real heat exchanger, the shellside flow enters through an inlet nozzle and, as shown in the computer generated plot of flow distribution at a particular cross-section, given in Fig. 3, the flow direction varies up to 45° with respect to the inlet flow direction. Consequently, a tube bundle specified as a 30° triangular layout bundle with respect to inlet flow may behave as a "60° triangular layout" in other portions of the tube bundle. The implication here is that the sensitivity of a given tube to flow direction, as studied by Yeung and Weaver,[5] must be kept in mind when interpreting the results from real heat exchanger tube bundle tests.

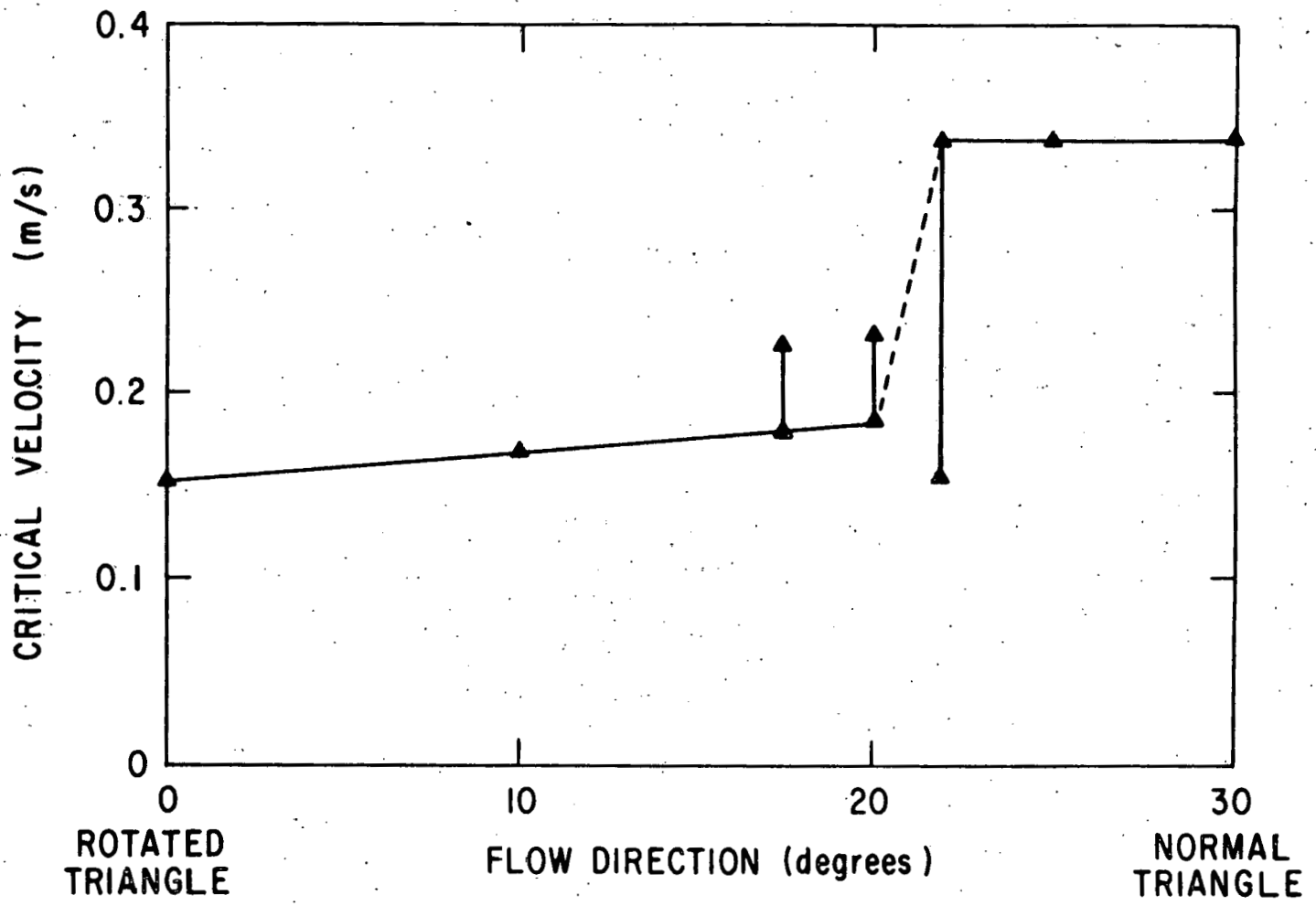

Fig. 2. Effect of incident flow direction on critical velocity [5]

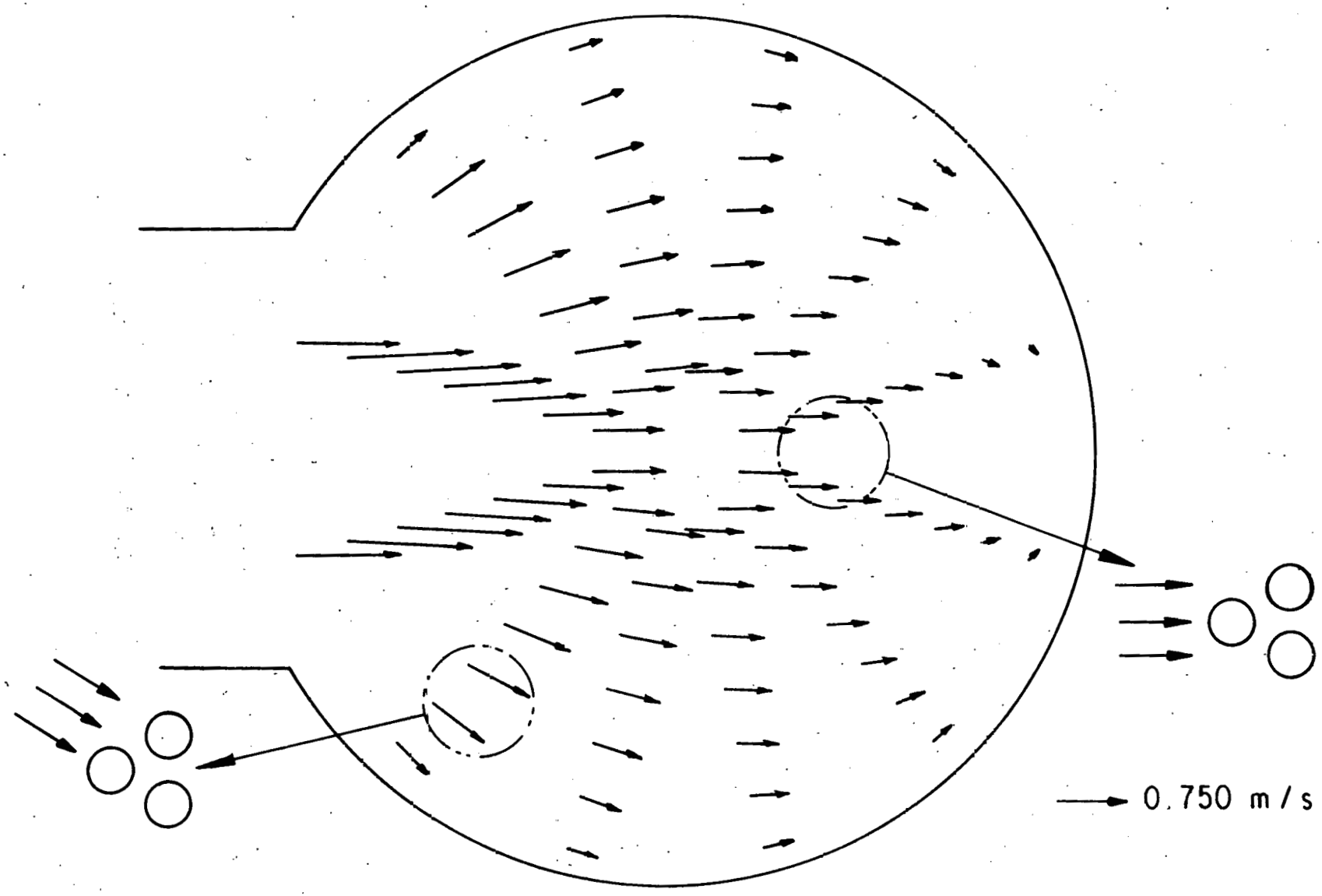

Fig. 3. Computer generated plot of flow distribution at a cross-section through the inlet nozzles

B. Criteria for Determining Critical Flow

As discussed by Chen,[3,4] and reviewed above, when the flow velocity through a tube array exceeds a threshold value, the fluid forces contributing to the modal damping are such as to cause the damping to become negative and the system to become unstable. When the flowing fluid is a liquid, the reduced flow velocity U_r (= U/fd) at which instability occurs is typically small (<15). The instability is caused by fluid damping forces and is called a "velocity mechanism" as the energy flow to the tubes is attributed to tube velocity. For gas flows, instability occurs at a large value of U_r. The fluidelastic force is dominant and the energy flow to the tube array is attributed to a "displacement mechanism"; phase difference among the tubes is an essential feature and fluidelastic coupling between tubes is a necessary condition. In the absence of impacting with adjacent tubes, a tube can be defined as undergoing fluidelastic instability if its motion occurs at a single, well-defined frequency (corresponding to the particular instability mode) and its amplitude is increasing with flow velocity at a relatively rapid rate.

The threshold flow velocity corresponding to the onset of instability is not always easy to determine in laboratory tests and is even more difficult to establish in the case of real heat exchange equipment. The situation involving a real heat exchanger is complicated by the large number of tubes in the bundle and the complex (nonuniform) flow distribution which will result in specific groups of tubes experiencing instability at a lower flowrate than other groups of tubes.

There are a number of methods that have been used to define the threshold flow for instability. These are reviewed below:

(1) Sensory Observations - In general, tube vibration amplitudes increase dramatically when the critical flowrate is reached, typically causing the tubes to impact with one another. Provided the tube bundle can be viewed from the end, the amplitude increase can generally be detected visually. If, in addition, tube impacting results, a distinctive loud noise associated with impacting is readily audible. The method is applied by increasing the flow in steps, or continuously at a slow rate, and observing the dynamic response of the bundle.

When the tubes are vibrating at sufficiently large amplitudes to cause audible impacting and/or permit visual observation of the tube

motion, there is little doubt that the tubes are experiencing fluidelastic instability. One disadvantage of this method is that it is somewhat subjective and requires a fair amount of engineering judgment and experience. A second disadvantage is that the results, so obtained, may not be conservative, considering that the tubes may have gone unstable, at moderate amplitudes without impacting, at a somewhat lower flow than that identified by observations. An obvious advantage is that the method is fast, easy to apply, and allows for surveillance of the entire bundle at one time.

The remaining methods to be reviewed each require instrumenting selected tubes with accelerometers or other motion sensing devices. Again, the flow is increased in steps or swept at a slow rate starting from a low value. In this case the response time histories are recorded on magnetic tape for subsequent data processing.

(2) Vibration Amplitude vs. Flow - Response Rate. The tube vibration response time histories are processed to obtain rms values of acceleration or displacement. The rms response is plotted as a function of flow velocity or flowrate as shown, for example, in Fig. 4. The flow velocity at which the tube experiences a rapid increase in response is defined as the critical flow velocity. Soper[6] defines the intersection with the velocity axis of the tangent to that portion of the curve which is rapidly rising as the critical flow velocity (see Fig. 4a).

The example given in Fig. 4a is ideal and there is no problem in defining the critical flowrate with this method. However, typically with water on the shellside the response versus flow curve may peak, drop off and then show a rapid rise. See, for example, Fig. 4b. There is uncertainty in such cases as to whether or not the first peak indicates instability. Problems in definition also arise in cases in which the rms response exhibits a gradual increase to a high level, as in Fig. 4c, rather than an abrupt increase, as in Fig. 4a. As in the first method, a certain amount of engineering judgment is required.

(3) Vibration Amplitude vs. Flow - Amplitude Threshold. To overcome the ambiguity in establishing the critical flow velocity for cases in which the rms response versus flow curves exhibit "undulations" and/or a gradual rise, several investigators have established a "threshold displacement amplitude." The critical flow velocity is defined as the velocity at which

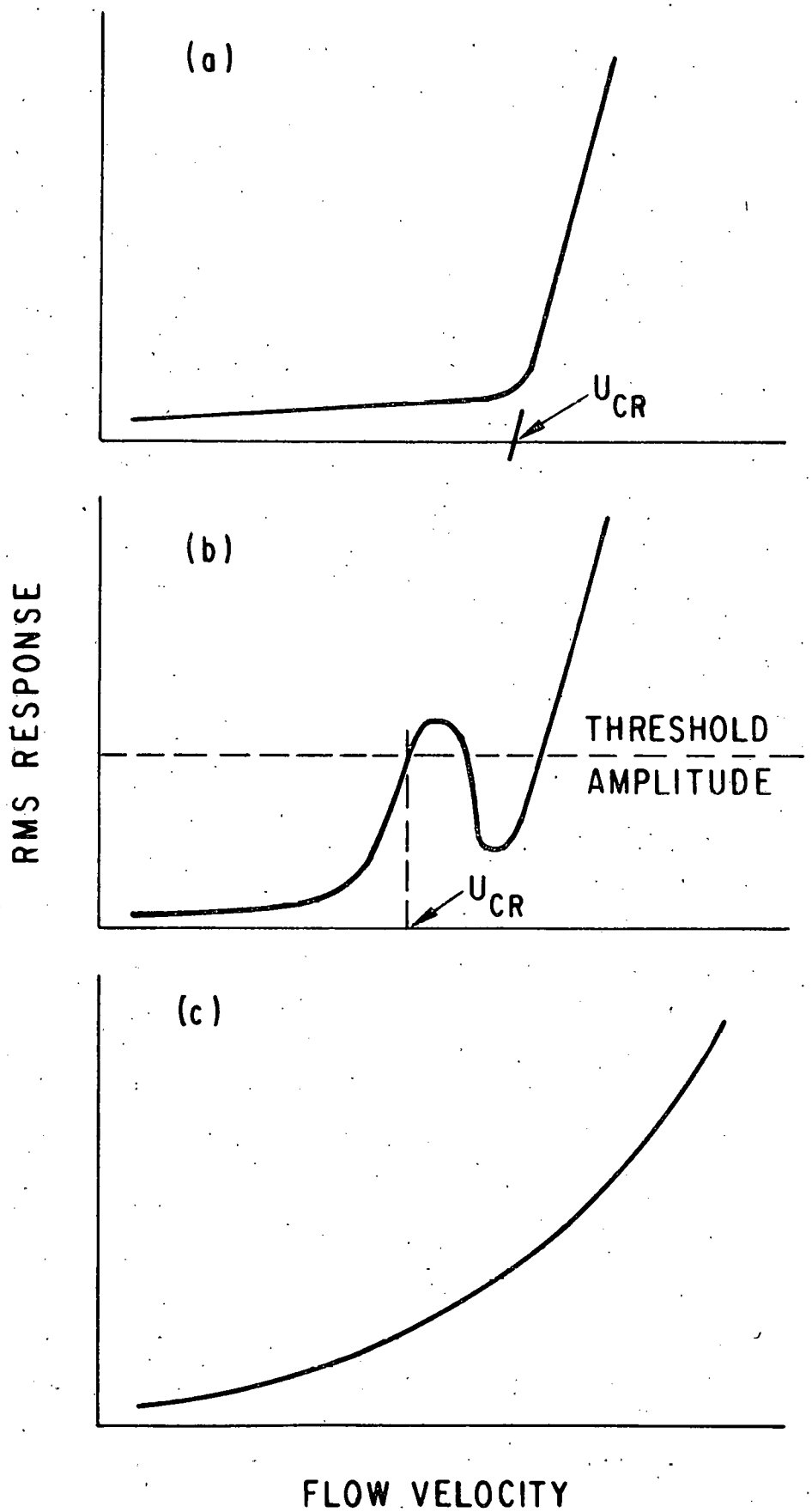

Fig. 4. RMS tube response versus flow velocity

the threshold displacement is first exceeded. Values of 2 to 2.5 percent of the tube diameter have been suggested.[5]

Once a threshold amplitude is established the method is straightforward in application, see Fig. 4b. However, again, engineering judgment is required in the selection and application of the criterion. See, for example, Ref. 5.

(4) Flow Sweep - Time History. A slow sweep up in flow is performed while tube acceleration time histories are recorded on magnetic tape. A careful examination of the time histories is carried out to determine the time (corresponding to a particular flow) at which large amplitudes suddenly occur. Peak amplitudes can be compared with the available "vibration space" to determine if impacting can be expected to be occurring. In application of this method the relationship of the mode shape relative to the axial location in the tube of the accelerometer must be considered. For example, as shown in Fig. 10, by virtue of the mode shape the peak response in one span can be significantly greater than that in an adjacent span. Therefore, if the accelerometer is located in a span with a smaller relative motion, analysis of the response peaks may indicate that impacting is not occurring whereas it may, in fact, be occurring in an adjacent span.

This method can be rather tedious and time consuming to apply. It too requires engineering judgment.

(5) Frequency Response Data. The critical flow velocity can be thought of as the flow velocity defining the transition from turbulent buffeting to fluidelastic instability. When a tube bundle is immersed in a dense fluid such as water, fluid structure coupling occurs which gives rise to a broad band of closely spaced frequencies, centered about what would be the natural frequency of an isolated tube in water. At flow velocities below the critical value, turbulent buffeting is the dominant excitation mechanism. It excites this broad range of coupled frequencies, as evident from the response power spectral density curves. On the other hand, the vibration at instability will typically be at a well-defined, single frequency (corresponding to the instability mode).

In application of this method, the vibration response time histories are processed on a Fast Fourier transform Analyzer to obtain power spectral density (PSD) representations of the data. The flow velocity (or flowrate) at which the response PSD changes from a relatively

broad-band spectrum to a narrow-band (single frequency) spectrum is defined as the critical flow velocity. See, for example, Fig. 5.

In general, this method is felt to be quite accurate and relatively precise. However, engineering judgment will still be required in situations in which the broad-band spectra associated with turbulent buffeting "narrow" significantly before becoming extremely sharp. Also, in cases in which the instability is very abrupt, the large amplitudes might initiate impacting which, in turn, will be represented as a broad frequency range on the PSD. In this case, it may cause one to miss the single frequency spike representative of instability.

Of these different methods, the last method, based on the transition from a broad-band turbulent buffeting response to a single-frequency response as defined by the shape of the frequency response spectra, is perhaps the most precise. It identifies the onset of instability regardless of the displacement amplitude. The other methods all tend to be more subjective and dependent on engineering judgment. In determining the critical flowrate in an industrial heat exchanger bundle it is usual practice to employ all the available methods and to compare the results from one against those from another. In particular, since it is practically possible to instrument only a small percentage of the large number of tubes in the bundle, it is necessary to rely on sensory observations to identify those tubes and groups of tubes that first experience large amplitude motion. Selected tubes, from those so identified, can then be instrumented, and one or more of the other methods, which are dependent on response data, can be applied to more accurately determine the onset and drop-out (with decreasing flow) of instability. This is the approach followed in the subject test program.

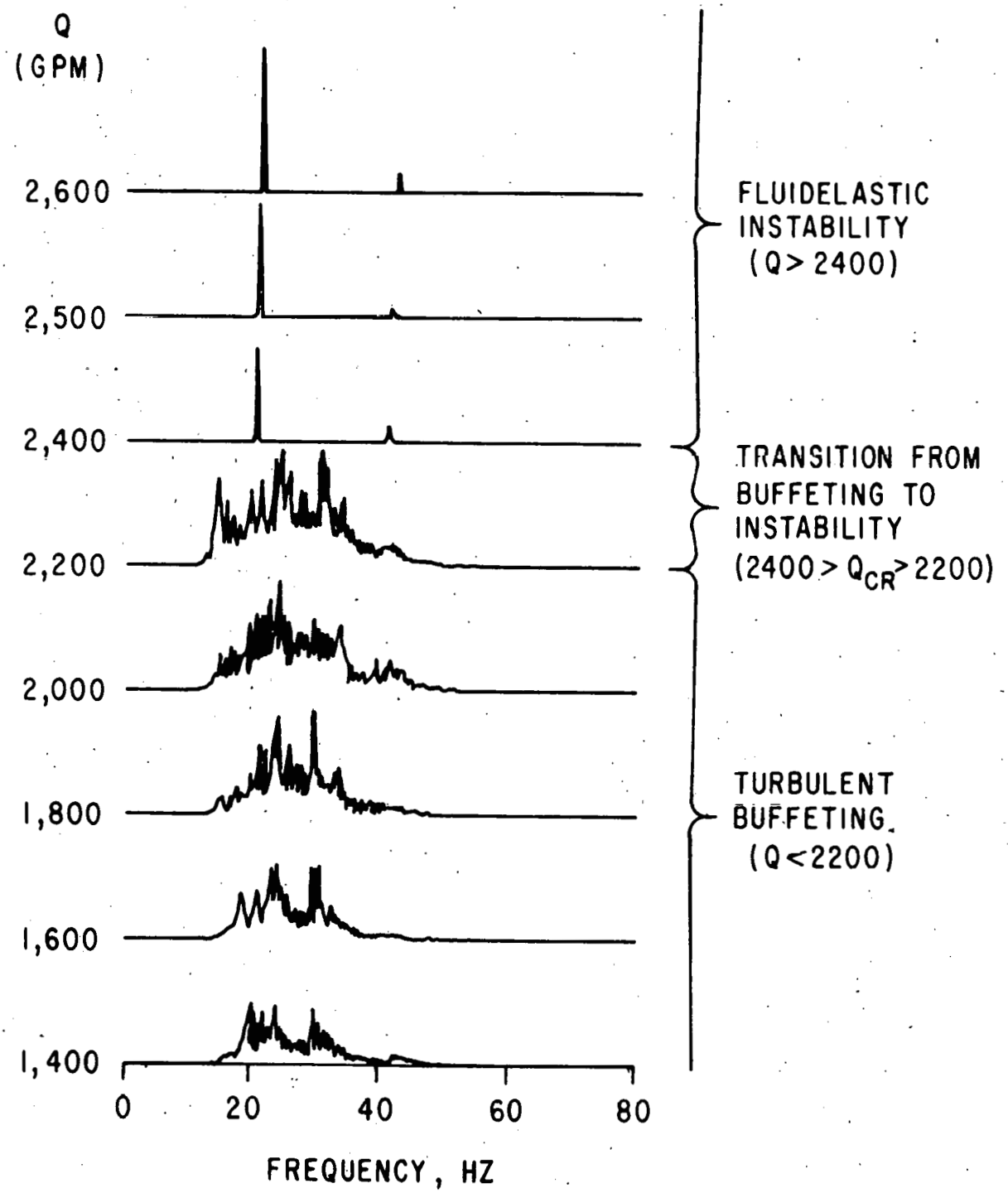

Fig. 5. Tube response PSDs for various shellside flowrates (ordinate not to scale)

III. TEST DESCRIPTION

A. Test Exchanger and Flow Facility

The test exchanger is a segmentally baffled shell and tube exchanger representative of an industrial heat exchanger, but specially designed to permit easy assembly/disassembly necessary to achieve different tube bundle configurations. For this series of tests, the exchanger is configured as a six crosspass (five equally spaced baffles) unit as shown schematically in Fig. 6. The general features and basic dimensions are given in Table 1. The exchanger is piped to Argonne's Flow-Induced Vibration Test Facility (FIVTF) as shown in Fig. 1. The FIVTF has four pumps which can be operated in combinations to deliver a maximum water flowrate of up to 0.50 m^3/s (8,000 gpm) to the shellside of the bundle. The tubes are left open.

Two sets of tubes are used in the testing. The one set consisted of smooth tubes of Admiralty brass with an outside diameter of 19.1 mm (0.75 in.) and a wall thickness of 1.2 mm (0.049 in.). The second set consisted of finned tube of the same material with lands where the tubes passed through the baffle plates. The finned tubes have an outside diameter of 19.1 mm (0.750 in.), a root diameter of 15.9 mm (0.625 in.), and an inside diameter of 13.8 mm (0.542 in.). There are 19 fins/in. with a nominal fin thickness of 0.64 mm (0.025 in.) and gap between fins of 0.97 mm (0.038 in.).

The tubes are arranged on a triangular layout (a so-called "30° orientation" with respect to the inlet nozzle flow), as shown in Fig. 7, with a pitch to diameter ratio of 1.25. There are 488 tubes in the bundle not counting the tie bars and tie bolts. The scheme adopted to identify tube location is also given in Fig. 7. The baffle cut is 28.9 percent of the diameter providing saddle-type support at alternate baffles for the tubes in rows H and T.

B. Test Cases

Ten different test cases were run as part of this test series. The test cases are defined by case numbers 6-15; case numbers 1-5 correspond to the eight crosspass tests and are reported in Ref. 2. The test cases are summarized in Table 2 and are briefly discussed below.

Test cases 6 and 7 were selected to obtain data that would permit evaluation of the effect of inlet/outlet nozzle size on tube bundle instability. Test cases 8-10 and 12 represent potential field fixes as

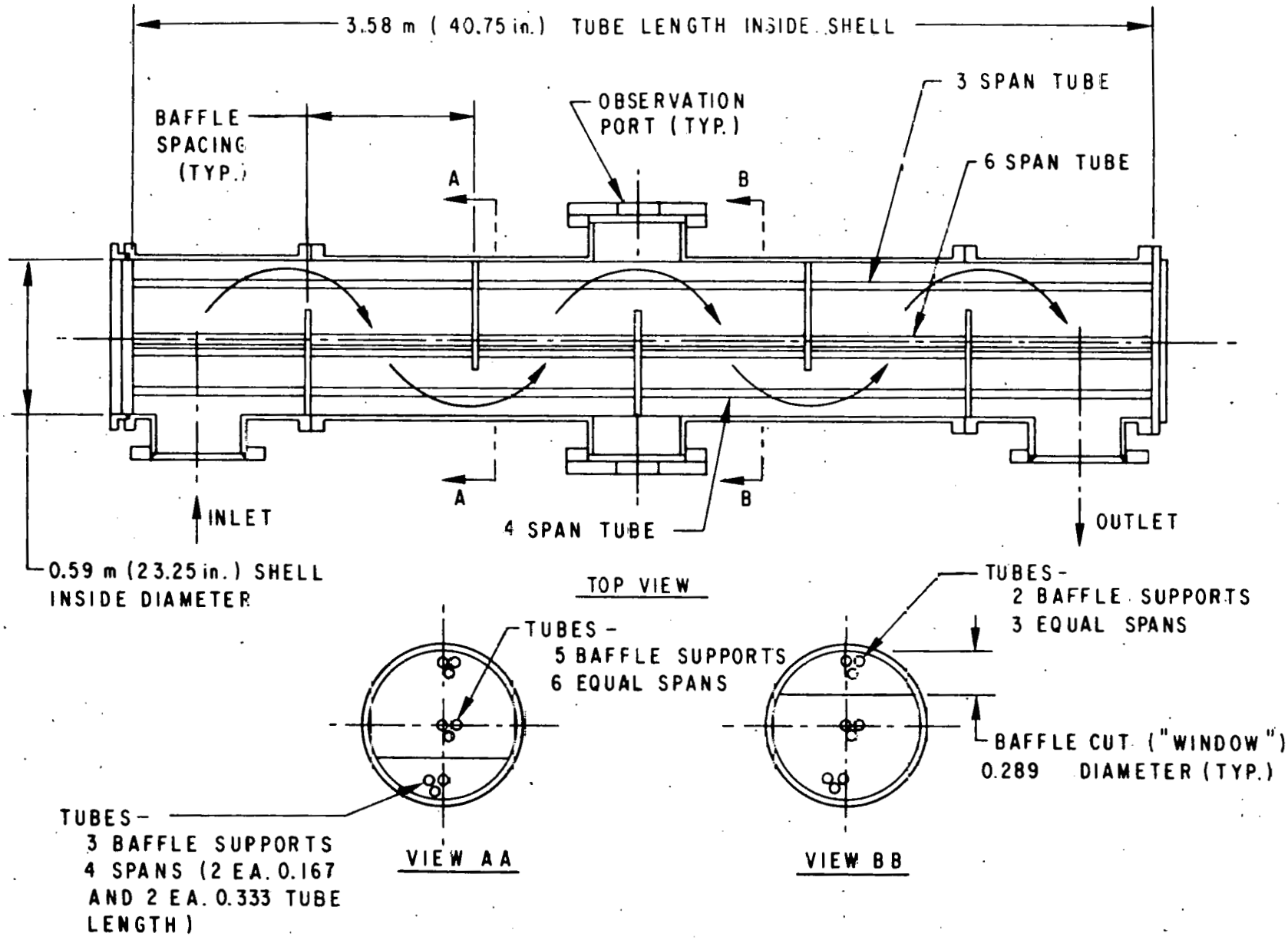

Fig. 6. Schematic of six-crosspass (five equally spaced baffles) configuration

Table 1. General features and basic dimensions of test exchanger

Shellside fluid	Water
Tubeside	No fluid, open tubes, ready insertion of instrumentation
Shell (Stainless steel), I.D.	0.59 m (23.25 in.)
Shell, inside length (tubesheet spacing)	3.58 m (140.75 in.)
Modular shell construction	Flexibility to change nozzle orientation
Nozzles	Insertion of piping to reduce inside diameter possible Maximum inside diameter: 0.34 m (13.25 in.)
Nozzles at shell midspan	Observation ports or alternate flow route (e.g., direct crossflow)
Tube bundle	Removable unit, ready assembly/ disassembly
Tubesheets	One stationary, one floating; special double tubesheet construction to contain O-rings to seal tubes
Tie bolts	Stainless steel rods in tube locations Secure and space tubesheets on both ends of heat exchanger Compress double tubesheets on each end to seal O-rings
Tie bars	Secure and space baffle plates

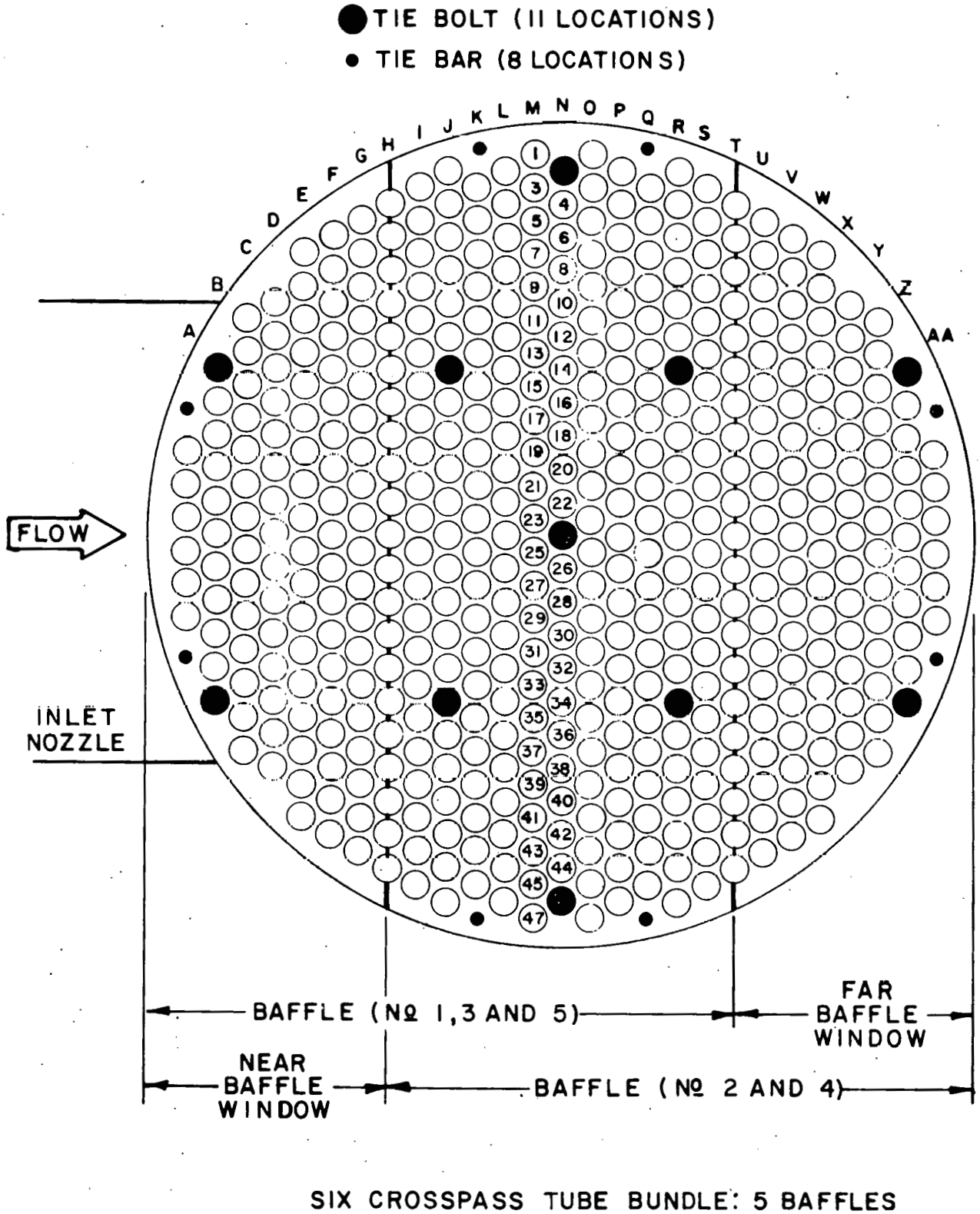

Fig 7. Tube layout and scheme for identifying tube location

Table 2. Summary of test cases

Case No.	Tube Bundle Configuration
6	Full bundle; 14 in. inlet/outlet nozzles
7	Full bundle; 10 in. inlet/outlet nozzles
8	Row U removed (Fig. 8a)
9	Row U replaced with stainless steel tubes
10	Pass lane in far window region (Fig. 8b)
11	Full bundle (rerun of Test Case 7)
12	Pass lanes in both window regions (Fig. 8c)
13	NTIW bundle (Fig. 8d)
14	NTIW bundle; finned tubes
15	Full bundle; finned tubes

Note: Test Cases 8-15 performed with 10 in. inlet/outlet nozzles

illustrated in Fig. 8. Since experience has shown that the first tube row past the baffle cut is most susceptible to fluidelastic instability, test cases were selected with that row removed (case 8, see Fig. 8a) and with that row replaced with stiffer (stainless steel) tubes (case 9). The effect of pass lanes is investigated in test cases 10 (pass lane in far window region, see Fig. 8b) and 12 (pass lanes in both window regions, see Fig. 8c). Heat exchanger designers resort to the no-tubes-in-window (NTIW) bundle (Fig. 8d) when it is required to ensure against a tube vibration problem. The NTIW bundle is very often employed in the large diameter units which are today becoming more common. Finally, test cases 14 and 15 employ finned tube bundles in full bundle (case 15) and NTIW (case 14) configurations.

C. Test Procedure/Data Processing

Prior to flow testing, natural frequency and damping measurements are performed on selected tubes in both the near- and far-window regions of the tube bundle. The measurements are made both in air and with still water on the shellside using a specially developed electrodynamic vibrator[2] that is inserted into the tubes.

As discussed earlier, it is practically not possible to instrument all 488 tubes in the bundle, or even the somewhat smaller number of tubes in the window regions that will be more susceptible to vibration by virtue of their lower natural frequencies. To gain insight to the overall dynamic behavior of a particular tube bundle, the initial flow test is typically performed without the tubes instrumented. The flow is increased in step changes and the tube bundle backlit to facilitate the visual detection of tube motion by sighting down the tube bores; large amplitude tube motion associated with instability is readily detected with this technique. The onset of instability can also be determined from the sudden increase in audible noise coming from the unit. From visual observation of the overall bundle response, the tubes first experiencing large amplitude vibration are identified. It is from this group that tubes are selected to be instrumented.

Subsequent flow tests are performed with selected tubes instrumented with miniature accelerometers. The accelerometers are mounted on specially designed plugs and are inserted into the tubes. The flowrate is increased in steps and at each step the acceleration-time signals are recorded on FM

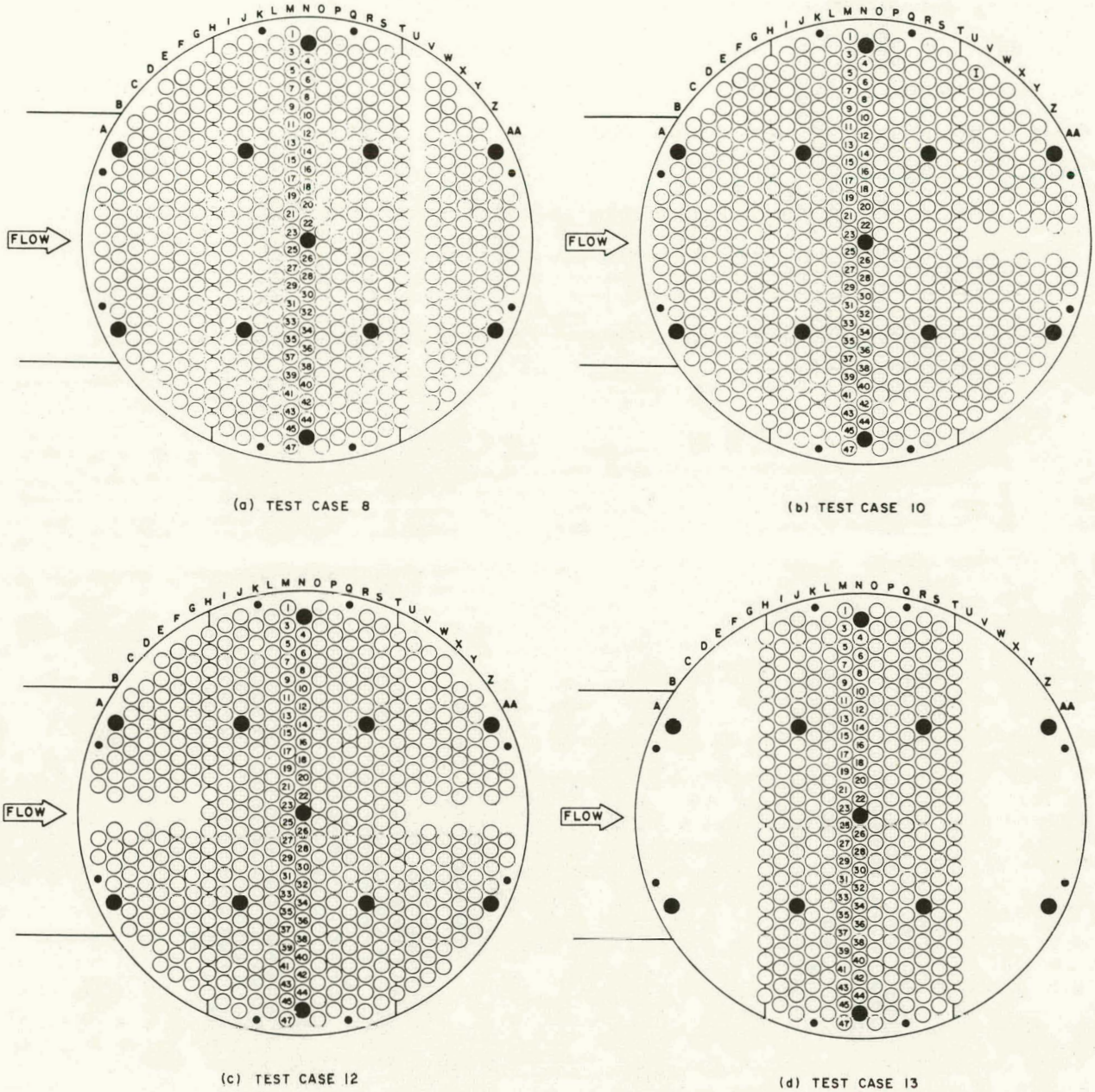

Fig. 8. Schematic representation of field fixes and NTIW configuration: (a) Test Case 8; (b) Test Case 10; (c) Test Case 12; (d) Test Case 13

magnetic tape. In some tests, slow "flow sweeps" are employed. In these cases both flowrate and tube acceleration are simultaneously recorded as a function of time.

The acceleration signals are then processed on a Fast Fourier Transform (FFT) Analyzer to obtain power spectral density (PSD) representations of the response and root-mean-square (rms) values. Corresponding displacement data is obtained by twice integrating the acceleration signals. The rms amplitudes, PSDs, and time-histories are used in application of the various methods, reviewed in Section II.B of this report, for determining critical flow.

In addition to the acceleration signals, pressures are measured at the shell inlet and outlet and at various locations on the shell wall. The locations of the pressure taps are given in a schematic in Fig. 9. The pressure measurements are taken after each incremental increase in flowrate.

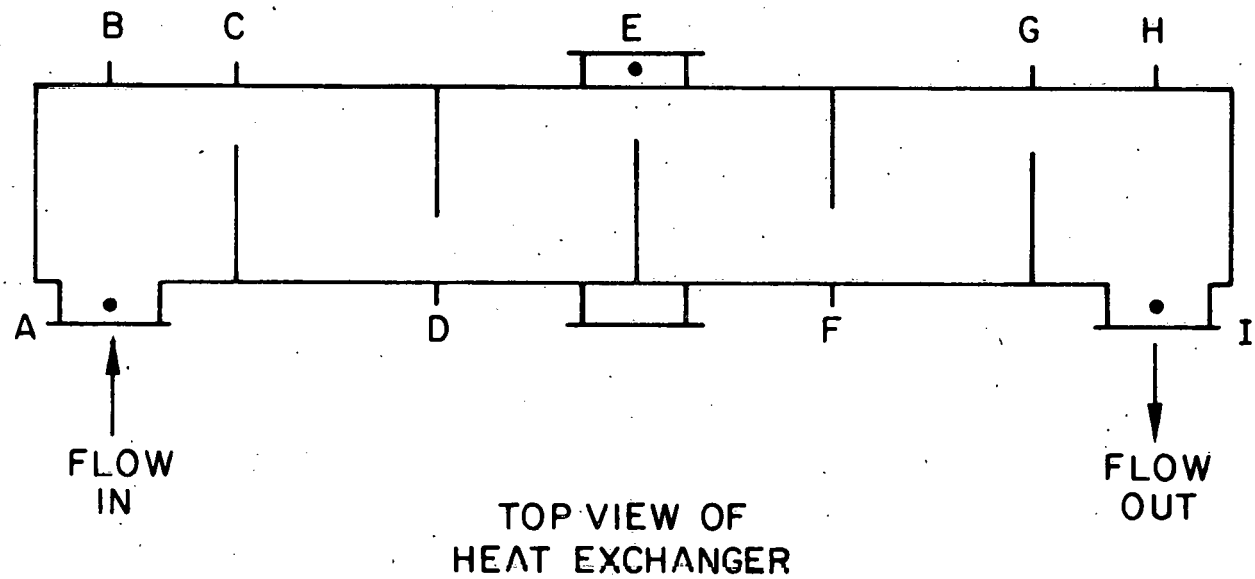

Fig. 9. Schematic showing locations of pressure taps

IV. NATURAL FREQUENCIES AND DAMPING

A. Theoretical Results

Tube natural frequencies and damping are determined by tube geometry, material properties, and supports. The tubes can be considered as uniform beams supported at their ends by the tubesheets and special O-ring seals, with intermediate support provided by the baffle plates. As there is clearance between the tubes and support holes, and, further, since the tubes are not perfectly straight, it is to be expected that the intermediate supports will vary from tube to tube as well as from one support to the next on a given tube. However, for the range of tube to baffle hole clearances typical of industrial heat exchangers, these variations in intermediate support are not expected to significantly effect tube natural frequency.[8]

As can be seen from Fig. 6, for a full tube bundle there are three different tube support configurations giving rise to 3-, 4-, and 6-span tubes dependent on a tube being supported by 2, 3, or all 5 baffles, respectively. The 3-span tubes are located in the so-called "far window" region of the bundle and the 4-span tubes in the "near window" region. There are actually two additional support configurations if one considers that the baffles are cut along the centerline of rows H and T and, consequently, these two rows have a special saddle-type support at alternate baffle locations; see Fig. 7.

The physical situation is that of a tube on multiple supports positioned within an array of closely spaced tubes, similarly supported. The entire bundle is immersed in a dense fluid. The natural frequencies of a tube with N spans will occur in groups of relatively closely spaced frequencies with N frequencies in each group. The effect of the dense fluid and close spacing of adjacent tubes will be to contribute to the virtual mass, thereby lowering the natural frequencies. An equally important effect is that the close spacing gives rise to fluid structure coupling which, in turn, results in coupled modes and closely spaced modal frequencies. Theoretically, if there are M tubes in an array, fluid structure coupling will result in 2M coupled frequencies corresponding to each uncoupled natural frequency. For an N span tube the number of frequencies occurring in a band is enhanced by the factor M to give a total of 2MN frequencies.

The natural frequencies and modes of a tube on multiple supports are readily clculated using a computer program developed specifically for that purpose.[9] Calculated natural frequencies are given in Table 3 for the first nine modes of the 3-, 4-, and 6-span tube configurations of the test exchanger. The corresponding modes are given in Fig. 10 for the 3- and 4-span configurations. The calculations are performed with the assumption that the tubes are fixed at the tubesheets. It can be readily observed from Table 3 that the frequencies occur in frequency bands (designated by the index i), with the number of frequencies in each band (designated by index j, j = 1, ..., N) equal to the number of spans for that tube. Because the 4-span tube has unequal span lengths, there is a subgrouping of frequencies within the basic grouping determined by number of spans. This is indicated by the dashed dividing line in Table 4. The in-water frequencies are based on an added mass correction factor of 1.714 which takes into account the proximity to surrounding tubes in the tube bundle but does not account for coupling with adjacent tubes (adjacent tubes are assumed to be rigid).

The coupled mode frequencies of a tube bundle are obtained by applying a method of analysis developed by Chen.[10] The method is based on potential flow theory. The coupled mode frequencies can be represented by the equation

$$f_{ijk} = \frac{f^{v}_{ij}}{\left(1 + \frac{\mu_k}{m}\right)^{1/2}} \qquad (4)$$

$i = 1, 2, 3, \ldots, \infty$

$j = 1, 2, 3, \ldots, N$

$k = 1, 2, 3, \ldots, 2M$

where N is the number of spans, M is the number of tubes in the array, and f^{v}_{ij} are the in vacuo frequencies of the multi-span tube, μ_k are the effective added masses per unit length, and m is the tube mass per unit length. Among other things, Chen has studied the effects of numbers of tubes on the upper and lower bounds of the effective added mass parameter. He has shown that for a tube in an equilateral triangular layout, the immediate "ring" of six tubes has the greatest influence on the coupling

Table 3. Calculated natural frequencies of test exchanger tubes

Mode No.	3-Span			4-Span			6-Span		
	i,j	f^v_{ij}	f^w_{ij}	i,j	f^v_{ij}	f^w_{ij}	i,j	f^v_{ij}	f^w_{ij}
1	1,1	30.9	19.2	1,1	32.1	20.0	1,1	104.0	64.8
2	1,2	45.2	28.2	1,2	46.9	29.2	1,2	123.8	77.1
3	1,3	54.7	34.1	1,3	105.3	65.6	1,3	150.9	94.0
4	2,1	110.0	68.5	1,4	128.5	80.0	1,4	180.8	112.6
5	2,2	135.0	84.1	2,1	179.1	111.6	1,5	207.0	129.0
6	2,3	150.9	94.0	2,2	187.9	117.1	1,6	218.9	136.4
7	3,1	237.2	147.8	2,3	246.0	153.2	2,1	402.0	250.4
8	3,2	273.5	170.4	2,4	280.5	174.7	2,2	440.1	274.1
9	3,3	296.0	184.4	3,1	404.5	252.0	2,3	489.1	304.7

f^v_{ij} = in-vacuo frequencies

f^w_{ij} = uncoupled, in-water frequencies

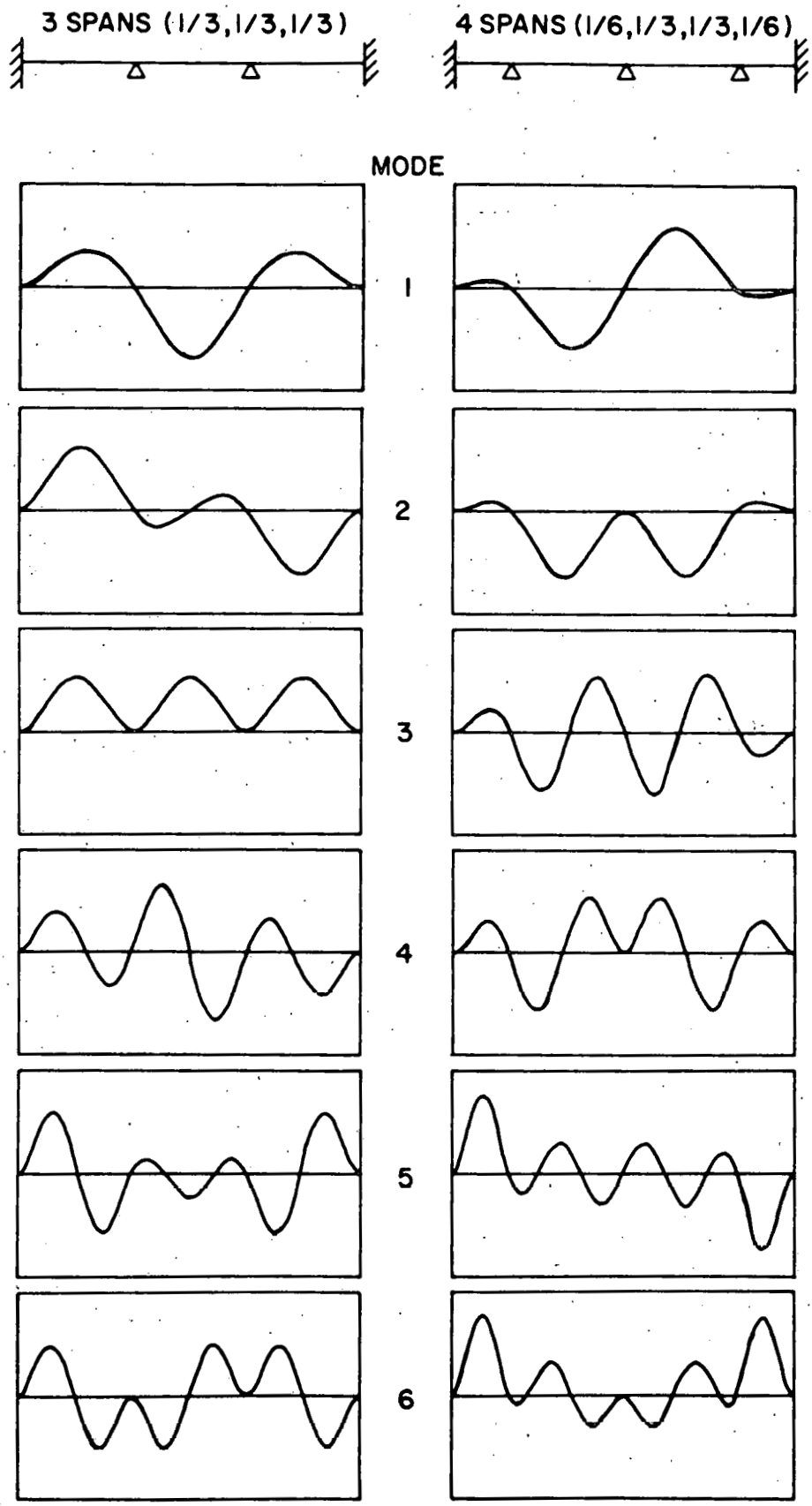

Fig. 10. Theoretical modes of 3- and 4-span test exchanger tubes

Table 4. Nondimensional effective added mass per unit length (Λ_k) for a triangular layout of 37 tubes with P/d = 1.25

k	Λ_k	k	Λ_k	k	Λ_k	k	Λ_k
1	0.294	20	0.516	39	1.325	58	2.832
2	0.318	21	0.532	40	1.325	59	2.889
3	0.318	22	0.574	41	1.344	60	2.929
4	0.346	23	0.574	42	1.496	61	2.940
5	0.346	24	0.616	43	1.500	62	2.940
6	0.370	25	0.660	44	1.500	63	3.023
7	0.371	26	0.692	45	1.791	64	3.023
8	0.399	27	0.692	46	1.791	65	3.083
9	0.401	28	0.703	47	1.877	66	3.083
10	0.401	29	0.767	48	2.136	67	3.110
11	0.416	30	0.767	49	2.136	68	3.204
12	0.417	31	0.870	50	2.267	69	3.242
13	0.417	32	0.875	51	2.428	70	3.327
14	0.437	33	0.875	52	2.429	71	3.327
15	0.437	34	0.880	53	2.504	72	3.471
16	0.438	35	0.972	54	2.636	73	3.471
17	0.480	36	0.972	55	2.636	74	3.596
18	0.480	37	1.099	56	2.679		
19	0.516	38	1.099	57	2.831		

and results from consideration of 19 and 37 tubes (the next two consecutive rings) do not vary significantly. In Table 4, the nondimensional parameter

$\Lambda_k \left(= \frac{\mu_k}{\frac{\pi}{4} \rho d^2}\right)$ is listed for a tube bundle of the test exchanger: triangular layout with a pitch to diameter ratio of 1.25. Three "rings" about a central tube are considered, i.e., M = 37.

For the smooth Admiralty brass tubes used in the test exchanger $\rho = 10^3$ kg/m^3 (0.0361 lb/in.^{3}), d = 19.1 mm (0.75 in.), and m = 0.597 kg/m (0.0335 lb/in.), to give

$$\frac{\mu_k}{m} = 0.476 \, \Lambda_k \quad . \tag{5}$$

Substituting Eq. (5) into Eq. (4) obtains

$$f_{ijk} = \frac{f_{ij}^v}{(1 + 0.476 \, \Lambda_k)^{1/2}} \quad . \tag{6}$$

The 3-span tube will theoretically have 222 (3 x 2 x 37) coupled mode frequencies in each frequency band while the 4-span tubes will have 296 (4 x 2 x 37) frequencies in each band. The maximum and minimum values of Λ_k are used to define the lower and upper bounds, respectively, for the frequency bands for each tube configuration. The lowest (first) frequency band is defined as

$$f_1^L = f_{1,1,1} \leq f_{1jk} \leq f_{1,3,74} = f_1^U \quad , \tag{7}$$

for the 3-span tube, and

$$f_1^L = f_{1,1,1} \leq f_{1jk} \leq f_{1,4,74} = f_1^U \quad , \tag{8}$$

for the 4-span tubes. Lower and upper bounds on the first frequency band can be calculated using the in vacuo frequencies given in Table 3 and values for Λ_1 and Λ_{74} from Table 4. Assuming the tubes are clamped in the tubesheet,

$$f_1^L = 18.8 \text{ Hz} \leq f_{1jk} \leq 51.3 \text{ Hz} = f_1^U \quad , \quad \text{for 3-span tube} \tag{9}$$

$$f_1^L = 19.5 \text{ Hz} \leq f_{1jk} \leq 120.4 \text{ Hz} = f_1^U \quad , \quad \text{for 4-span tube} \tag{10}$$

$$f_1^L = 63.1 \text{ Hz} \leq f_{1jk} \leq 205.1 \text{ Hz} = f_1^U \quad , \quad \text{for 6-span tube .} \qquad (11)$$

At flowrates below critical, the random excitation associated with turbulent buffeting will excite a large number of frequencies within the first frequency band.

B. Test Results

In air natural frequencies and damping are determined from PSD curves of tube acceleration response to excitation provided by a specially designed electromagnetic exciter which can be inserted into the tubes.[2] Results from three typical tubes (two 3-span tubes, U-5 and U-23; and a 4-span tube, A-23) are given in Table 5, where they are compared with the theoretical results from Table 3. The agreement between measured and theoretical results is very good thus providing confidence in using theoretical results in analysis of the tube bundle.

Damping cannot be calculated and is inherently difficult to measure. Nevertheless, damping estimates can be obtained from the frequency response curves using a bandwidth method. In air results obtained by this technique are given in Table 6 for three typical tubes U-5, U-23, and A-23.

Attempts were made to measure natural frequencies and damping in water. However, because of the large number of closely spaced frequencies that result from fluid structure coupling, these measurements were difficult to interpret. To minimize the coupling with adjacent tubes, the tubes surrounding the instrumented tube were weighted and measurements were made under these conditions. The results obtained via this approach are given in Table 7 for three typical tubes from the test exchanger. The measured frequencies can be compared with the calculated values given in Table 3; the agreement is only fair.

Table 5. Comparison between measured and theoretical natural frequencies, f^V (Hz)

Mode No.	3-Span			4-Span	
	Theor.	U-5	U-23	Theor.	A-23
1	30.9	32	26,35	32.1	32
2	45.2	41	40,45	46.9	46
3	54.7	53	53	105.3	110
4	110.0	111	103	128.5	131
5	135.0	131	117	179.1	175
6	150.9	148	140	187.9	180
7	237.2	238	236	246.0	244
8	273.5	265	256	280.5	269

Table 6. Measured values of equivalent viscous damping factor, ζ^V

Mode No.	3-Span		4-Span
	U-5	U-23	A-23
1	0.016	-	0.009
2	0.007	0.012 - 0.017	0.006
3	0.005	0.004	0.005
4			0.003

Table 7. Measured values of natural frequencies f^w and equivalent viscous damping factor ζ^w

Mode No.	U-5		U-23		A-23	
	f^w	ζ^w	f^w	ζ^w	f^w	ζ^w
1	26	0.046	26	0.039	26	
2	35	0.015	37	0.025	44	0.018
3	43	0.010	44	0.023	82	0.008
4	92		80		93	0.009
5	114		92		122	
7	133		106		138	

V. FLOW TESTS

Flow tests were performed with the primary objective of obtaining tube bundle vibration information. However, as there is a lack of pressure drop data for heat exchangers, a secondary objective is to also obtain pressure drop information from the flow testing. Tube bundle vibration and pressure drop data are presented and discussed below.

A. Tube Bundle Vibration

The flow tests were performed following the test procedure outlined in Section III.C, and using the various criteria discussed in Section II.B to determine the threshold flowrate. Sensory (sight, sound, feel) observations are documented in the Appendix for each of the test cases. Based on these observations, the lowest critical flowrate for a given bundle configuration (test case), and the flowrate at which instability ceases, as flowrate is decreased, are determined. These results are summarized in Table 8.

Subsequent to the initial test run, in which observations are made and recorded, a select number of tubes from locations observed to be experiencing large amplitude vibration are instrumented with accelerometers. In subsequent test runs, these acceleration signals are recorded and analyzed to provide additional data that, among other things, are used to evaluate the conclusions arrived at from observations.

In the following, sensory observations made during the flow tests are summarized for each test case, and vibration response data in the form of rms values and/or frequency spectra are presented and discussed. Flowrate is given in gallon/min (gpm); the applicable conversion to SI (metric) units is 1 gpm = 6.3×10^{-5} m^3/s.

CASE 6

Case 6 is a 5-baffle, 6-crosspass full tube bundle configuration with 14 in. diameter inlet/outlet nozzles. Table 9 and Figs. 11-13 present pertinent data. The tubes most susceptible to instability were located in the central region of tube rows U and V adjacent to the baffle edge in the far window region opposite the nozzles. There the onset of instability occurred in the range of 1980 to 2140 gal/min. Frequency response curves of tube U-23 are given on Fig. 11, here the instability had not yet initiated at the 2090 gal/min flowrate. It is seen that the vibration frequencies increase with flow and that multiple frequencies are excited when the

Table 8. Critical flowrates from sensory observations

Test Case	Tube Bundle Configuration	Lowest Critical Flow Rate (gal/min)	Instability Dropout Flow Rate (gal/min)
6	Full - 14 in. nozzles	1980	1760
7	Full - 10 in. nozzles	1970	1880
8	Row U removed	1700	1450
9	Row U stiffened	2450	~1800
10	Pass lane - far window	2600	~2300
11	Full - 10 in. nozzles	2140	1700
12	Pass lane - both windows	2870	2500
13	NTIW	—	—
14	NTIW - finned tubes	—	—
15	Full - finned tubes	~2200	

Table 9. Flowrates initiating and ceasing instability at various full tube bundle locations

	Location of Tubes Affected (Refer to Fig. 7)	Flowrate (gal/min) Case 6 14 in. nozzles	Case 7 10 in. nozzles
Start of instability (severe vibrations) upon increasing flow	Far window (opposite nozzles) - central region	1980*	1970
	Far window - near shell periphery	2090	2130
	Near window	2320**	2790
Ceasing of severe vibrations upon flow reduction	Near window	2510	2500
	Far window - near shell periphery	2010	1880
	Far window - central region	1760*	1910

* Low values presented, additional runs indicated higher flowrates

** Was 2790 gal/min during an additional run

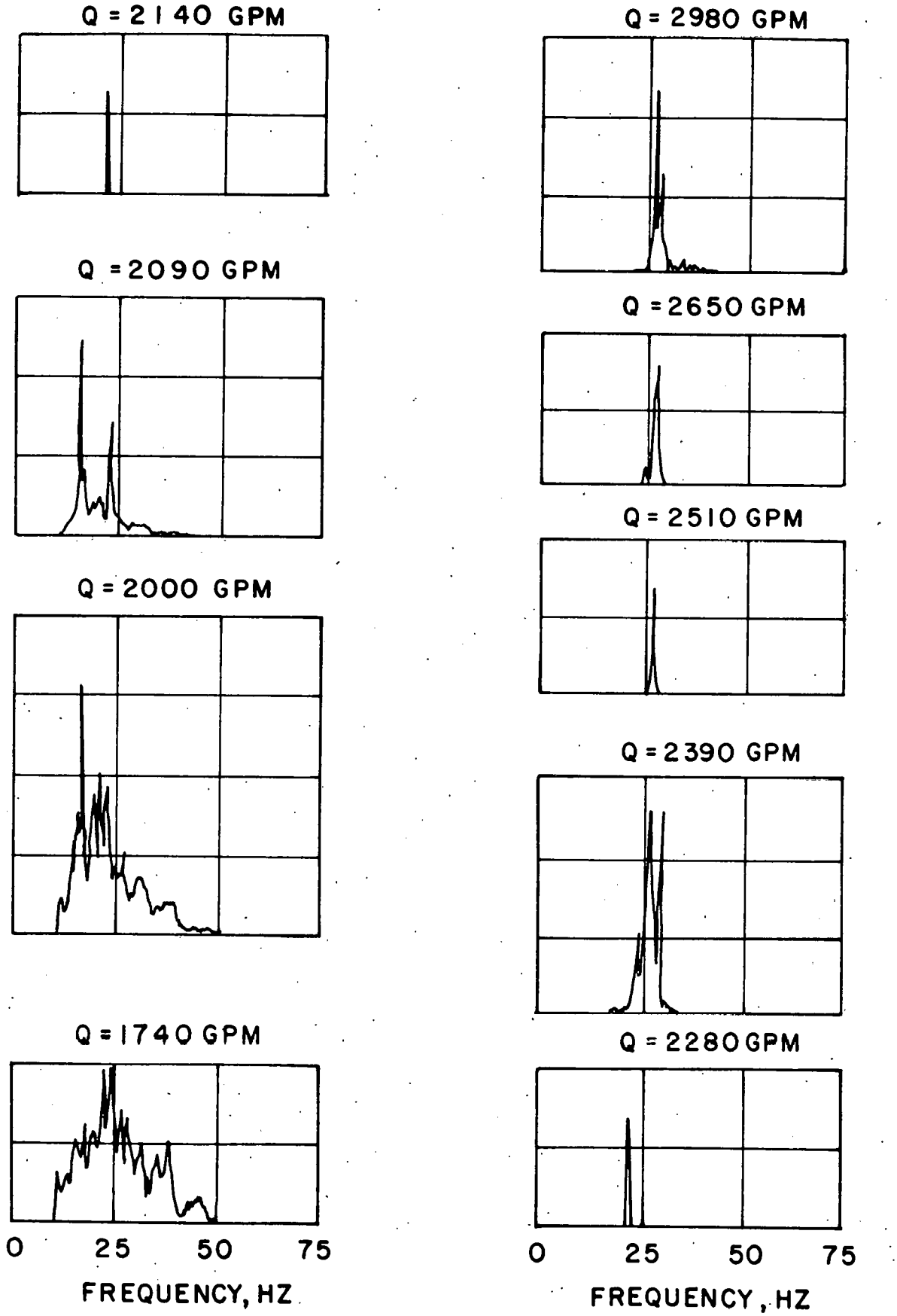

Fig. 11. Frequency response curves; Case 6, Tube U-23

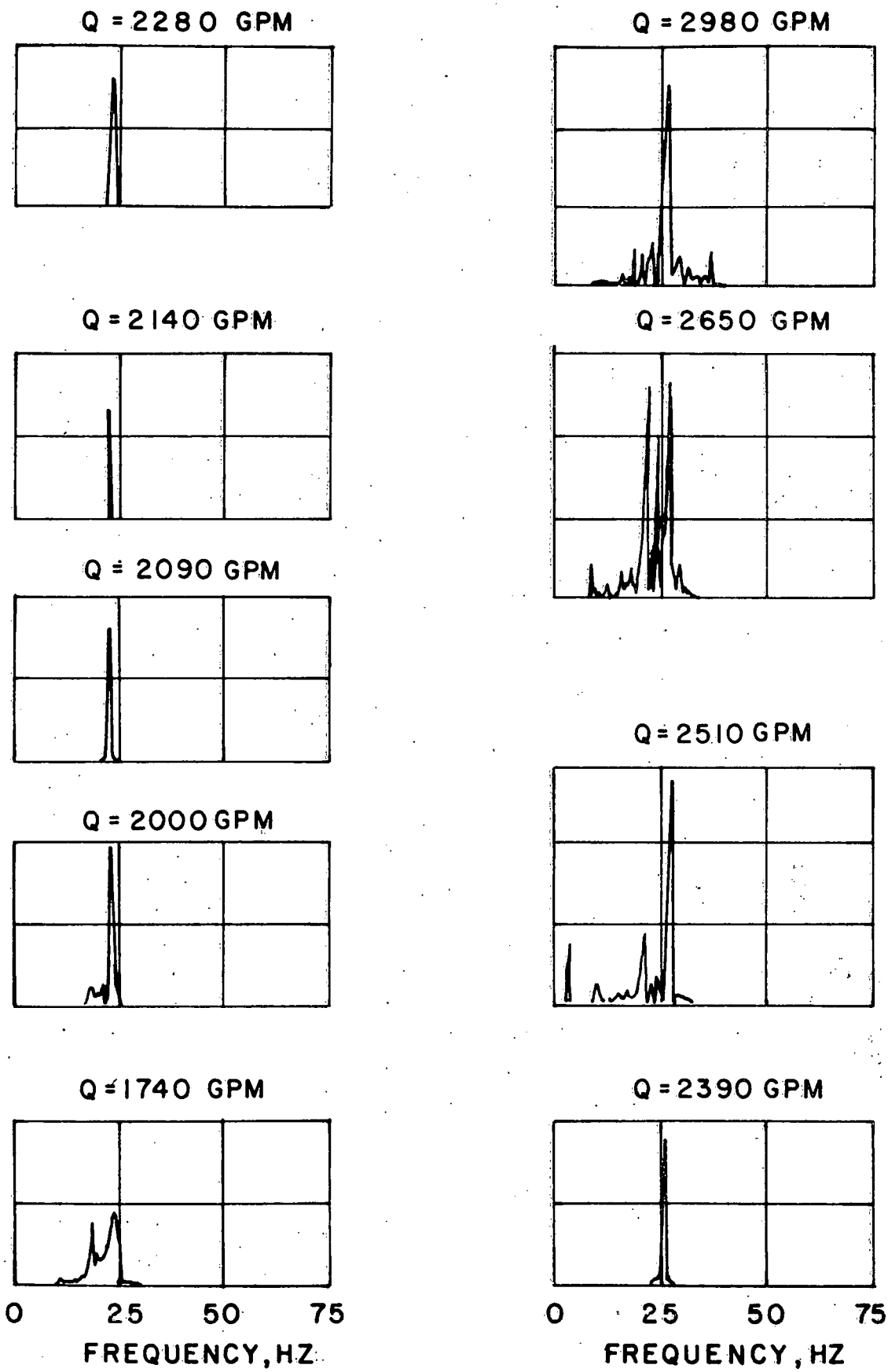

Fig. 12. Frequency response curves; Case 6, Tube V-42

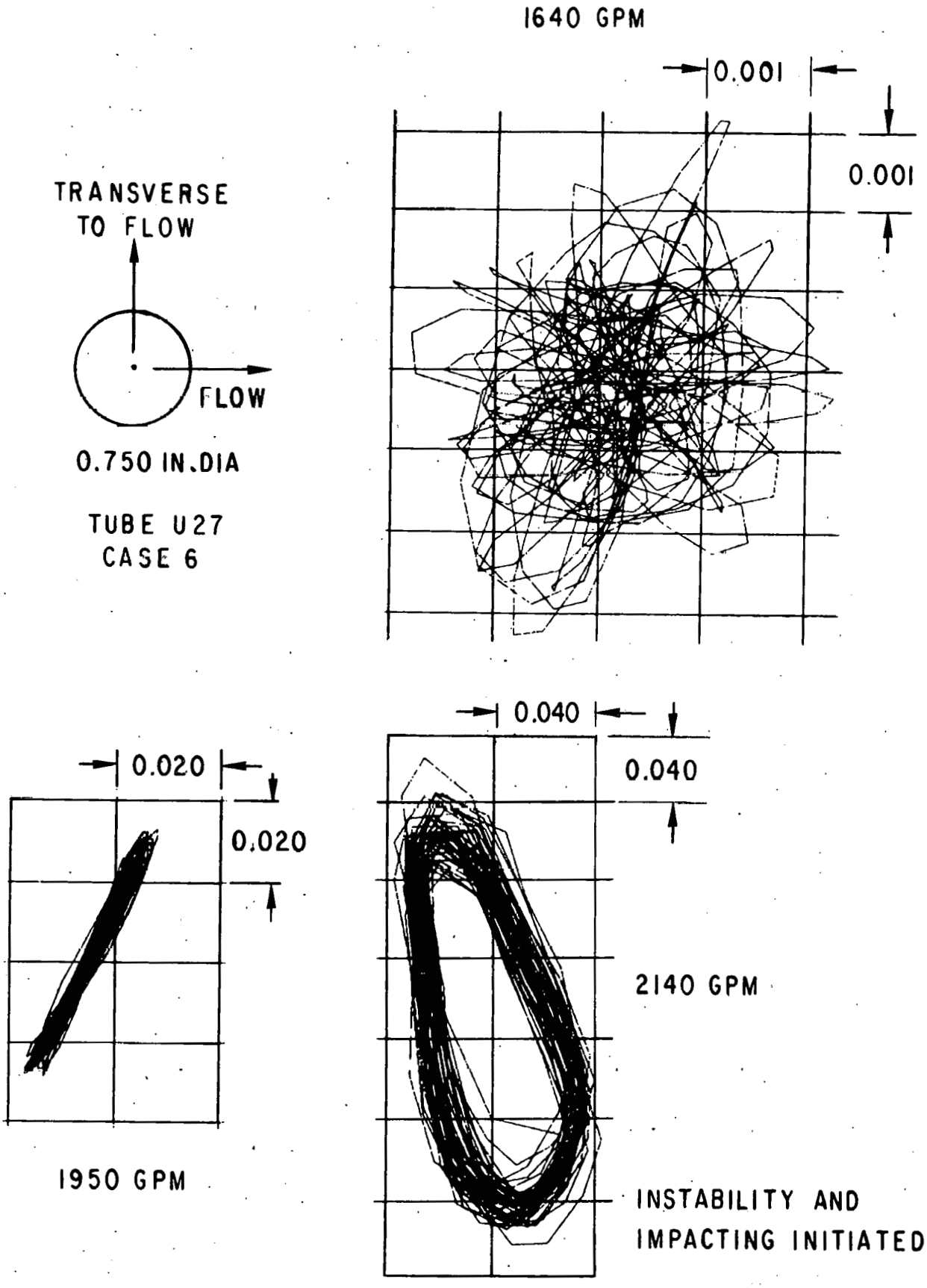

Fig. 13. Tube vibration patterns

tube impacts more violently with neighboring tubes at high flowrates. Vibrations with "beating" contribute "sidebands" on the spectra. The vibration performance was also investigated with another nearby tube U-27, which was instrumented with two biaxial accelerometers. Depending on the flow ranges, this tube was excited into different vibration patterns: random (more or less), straight line vibrations in lift or drag direction, and whirling. Some representative patterns are presented on Fig. 13. Even though the tubes in the row next to the baffle cut in the "far" window opposite the nozzle appear to be the ones most susceptible to instability, almost all the tubes in that window are vibrating sufficiently to be readily observed by eye. The tubes near the internal shell surface indicated a more gradual increase of vibration amplitude with flow rate, while the onset of the instability of the central tubes was abrupt. The frequency response of tube V-42 near the shell periphery is shown on Fig. 12, these data were taken during tests corresponding to those of Fig. 11. Flowrates to 3000 gal/min were applied. In the "near" window, on the side of the nozzles, substantial tube vibration activity began at the higher flowrates, particularly in the row next to the baffle cut where tube-to-tube impact occurred. However, no significant excitation of the row A tubes immediately exposed to the flow emerging from the nozzle was observed.

Upon flow reduction, various amounts of hysteresis were encountered as indicated on Table 9. Before and after instability, the vibration amplitudes were small.

CASE 7

Case 7 is a 5-baffle, 6-crosspass, full tube bundle configuration with 10 in. diameter inlet/outlet nozzles. The case 7 testing with the 10 in. nozzles provided results that were not much different from the Case 6 testing with the 14 in. nozzles. The lowest critical data fell into a slightly narrower range, 1970 to 2070 gal/min and also indicated smaller hysteresis effects (Table 9). At high flowrates there was a lot of vibration activity of the tubes above the top and below the bottom of the inlet nozzle where the flow appeared to bypass around the bundle along the inner shell surface. Although flowrates to 3250 gal/min were applied no significant excitation of row A tubes was observed.

Some fairly typical vibration amplitudes and principal frequency data obtained from tubes U-27 and V-42 are presented on Fig. 14. Different

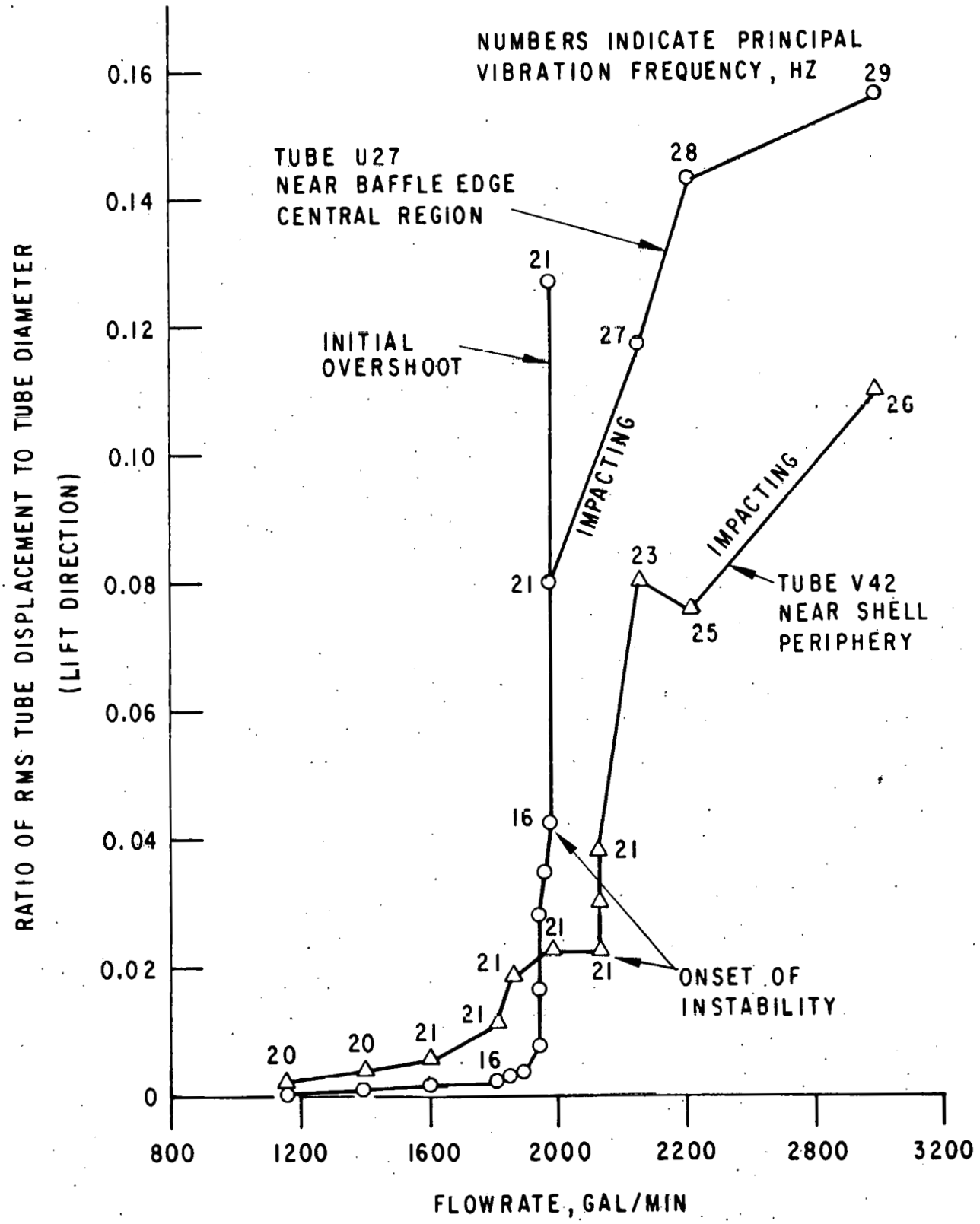

Fig. 14. Tube displacement vs. flowrate; Case 7, Tubes U-27 and V-42

amplitudes at the same flowrate were obtained at different points in time, usually only seconds apart.

In an effort to capture the motion of a group of tubes vibrating as the result of fluidelastic instability, a series of high-speed movies was taken at different flows with the bundle backlighted and opaque plastic plugs, with a very small aperture, located at midspan of 15 tubes. The movies dramatically show the difference in tube motion in successive rows. While the motion in the first row beyond the baffle cut in the far window appears to be primarily in a lift direction, the motion in the second row demonstrates considerable drag-direction motion. There are random changes in patterns as the flowrates increase, which indicate the impacting of adjacent tubes.

CASE 8

Case 8 is a 5-baffle, 6-crosspass with 10 in. diameter inlet/outlet nozzles having no tubes in row U. This was the first of a series of test configurations provided to simulate fixes that might be applied by operation in the field in order to increase the critical flowrate. For case 8, the seemingly straightforward approach was to remove the tubes most susceptible to vibration. Thus the tubes in row U next to the row saddled in the baffle cut were removed from the otherwise full tube bundle configuration. The vacated holes in the tubesheets were plugged, the holes in the baffles left open. Repeated flow testing indicated that this fix did not accomplish the desired result, on the contrary the critical flowrate was reduced to 1700 gal/min from 1970 gal/min for the full tube bundle. The instability initiated in tube row V next to the row vacated. "Hysteresis" kept the instability in effect until the flowrate was reduced to about 1450 gal/min. Since this "fix" only aggravated an existing problem, it is certainly one to be avoided.

CASE 9

Case 9 is a 5-baffle, 6-crosspass configuration with 10 in. diameter inlet/outlet nozzles and row U replaced with type 304 stainless steel tubes (3/4 in. o.d., 1/16 in. wall thickness). The stainless steel tubes were inserted without disturbing the tube bundle. The stainless steel tubes have natural frequencies 1.4 times greater than the Admiralty brass tubes.

Based on the sensory observations (Appendix - Case 9) made during an initial flow test, the critical flowrate for fluidelastic instability was

identified to be 2450 gpm. The tubes most susceptible to instability were determined to be located in the two rows (U and V) past the baffle cut in the far window region. General large amplitude vibration occurred in the far window region for flowrates in the range 2530 to 2600 gpm and above. Instability dropped out when the flowrate was decreased to 1850 to 1740 gpm.

To gain further insight into the dynamic behavior of the tube bundle and, more specifically, to determine if the row U tubes were "locking on" to the row V tubes, or vice versa, adjacent tubes in rows U and V were instrumented with accelerometers, inserted from the inlet tubesheet approximately 27 in. into the tube. In particular, tubes U-23 and V-24, along with tube C-15 from the near window region, were selected. A second test run was made and, for a range of flowrates (1400 to 2600 gpm), acceleration-time histories were measured and analyzed to obtain frequency response spectra (PSDs) and rms values. Frequency response curves are given in Fig. 15 for tubes U-23 and V-24, and in Fig. 16 for tube C-15; it should be noted that analyzer channels corresponding to frequencies in the range 55 to 65 Hz were cleared out to eliminate 60 Hz electrical noise present on some transducers.

For flowrates below the critical flowrate, viz., flowrates in the range 1400 to 2200 gpm, the frequency response curves of Fig. 15 clearly show that a broad range of frequencies are excited by the broad-band buffeting forces associated with turbulent flow through the bundle. The curves also indicate that between flowrates of 2200 and 2400 gpm there is a transition from a turbulent buffeting type of response (broad spectrum) to an instability (single-frequency) mode response. The precise flowrate at which this transition occurs is defined as the critical flowrate; better resolution (smaller increments) of flowrates would be required to accurately determine the critical value. The harmonics of the lowest frequency, occurring during instability ($Q > 2400$ gpm), are indicative of an impacting phenomenon taking place. In Fig. 15c results from tubes U-23 and U-24 are superimposed. This superposition clearly illustrates that at flowrates below the critical, the frequency band in which the stainless steel tube (U-23) responds is higher in absolute value (shifted to the right) than the response frequency band for the Admiralty brass tube (V-24). This result is expected since the in-vacuo natural frequencies of the

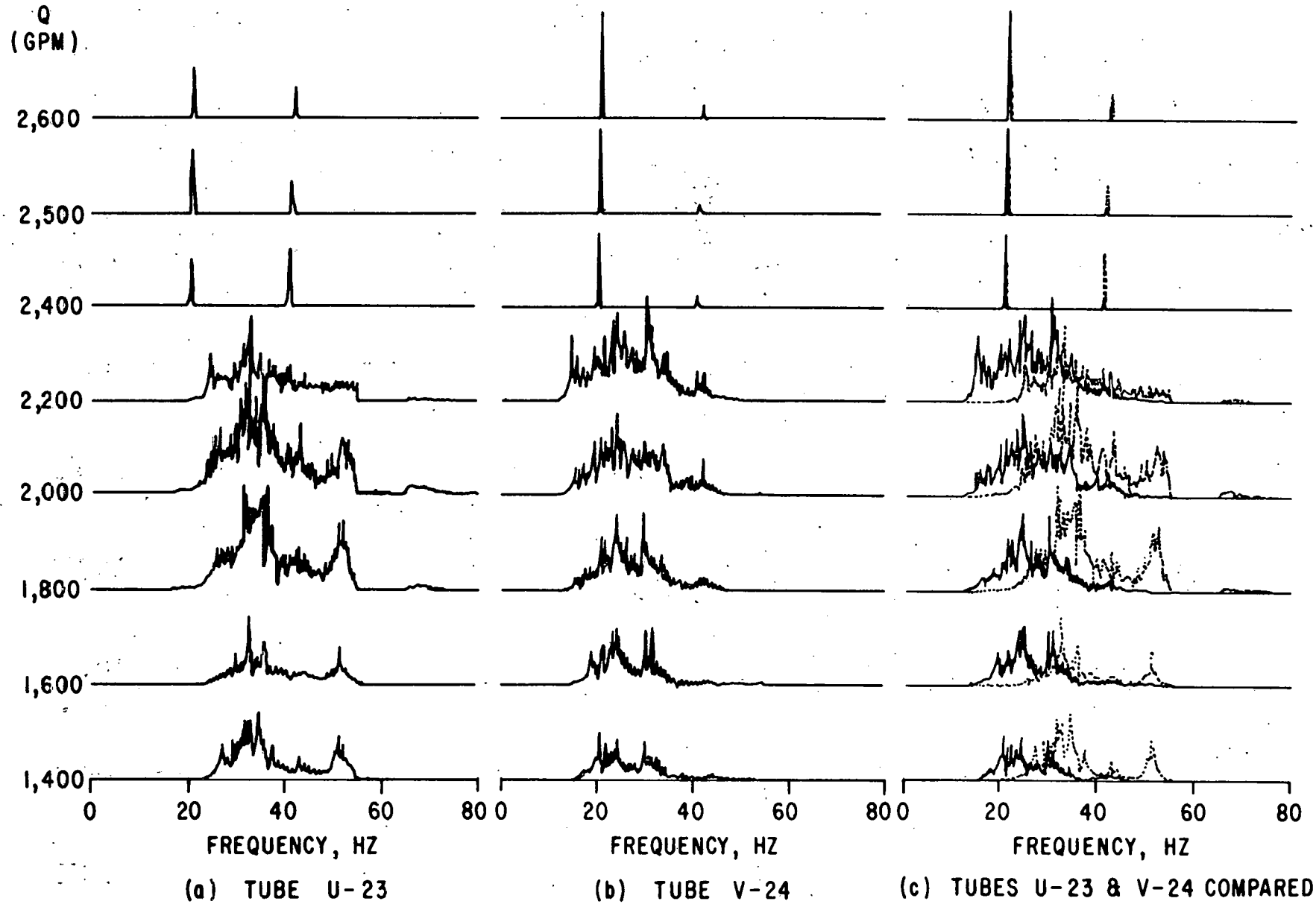

Fig. 15. Frequency response curves (a) Tube U-23, (b) Tube V-24, (c) Tubes U-23 and V-24 compared

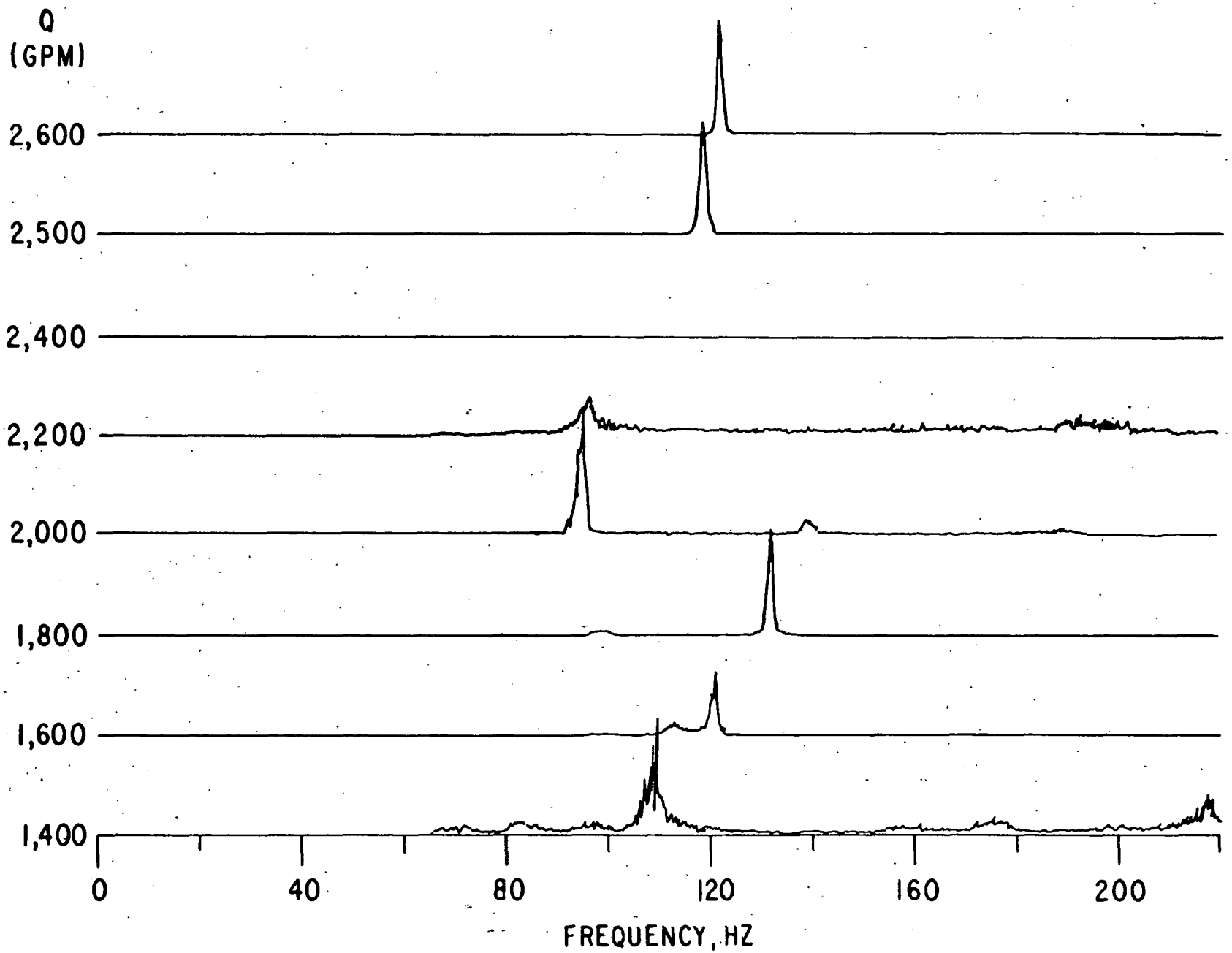

Fig. 16. Frequency response curve; Tube C-15

stainless steel tubes are correspondingly greater than the natural frequencies of the brass tubes. However, during instability, the instability mode frequency of the two tubes is identical; the tubes apparently are vibrating in a coupled mode.* At a flowrate of 2400 gpm the instability mode frequency is 20.1 Hz. As can be observed from Fig. 15, this frequency increases slightly with increasing flowrate.

In Fig. 16, the frequency response spectra from tube C-15, a 4-span tube, show that that tube responds at higher frequencies and that the dominant frequency at which it responds "moves around." The higher frequency response agrees with observations arrived at by touching the ends of the tubes with a finger. The response, although narrow band, is not sufficiently sharp to conclude that the tube was experiencing fluidelastic instability at any of the flowrates tested.

Curves of tube rms acceleration response versus flowrate are given in Fig. 17, as obtained from the frequency range 0 to 250 Hz. The abrupt increase in response of tubes U-23 and V-24, as the flowrate is increased from 2200 to 2400 gpm, indicates that the instability occurred in that flow range. This result agrees with that arrived at from a consideration of the frequency response spectra of Fig. 15. The rms acceleration response of tube C-15 shows a gradual increase. While the rms acceleration of tube C-15 is generally greater than that of tubes U-23 and V-24, the displacement will generally be smaller because of the frequency squared relationship between acceleration and displacement and the fact that the frequencies at which tube C-15 are responding are significantly greater than those of tubes U-23 and V-24.

Sensory observations made during the first test run indicated a lowest critical flowrate of 2450 gpm as given in Table 8. However, the results from a second test run using acceleration response data indicated that tubes U-23 and U-24 first experienced instability in the flow range of 2200 to 2400 gpm. Since impacting during instability is indicated by the presence of harmonics in Fig. 15, it would be expected that the instability is violent enough to be audible. Consequently, the disagreement between

---

*This type of behavior was also observed by Chen and Jendrzejczyk[11] in tests of bundles of curved tubes.

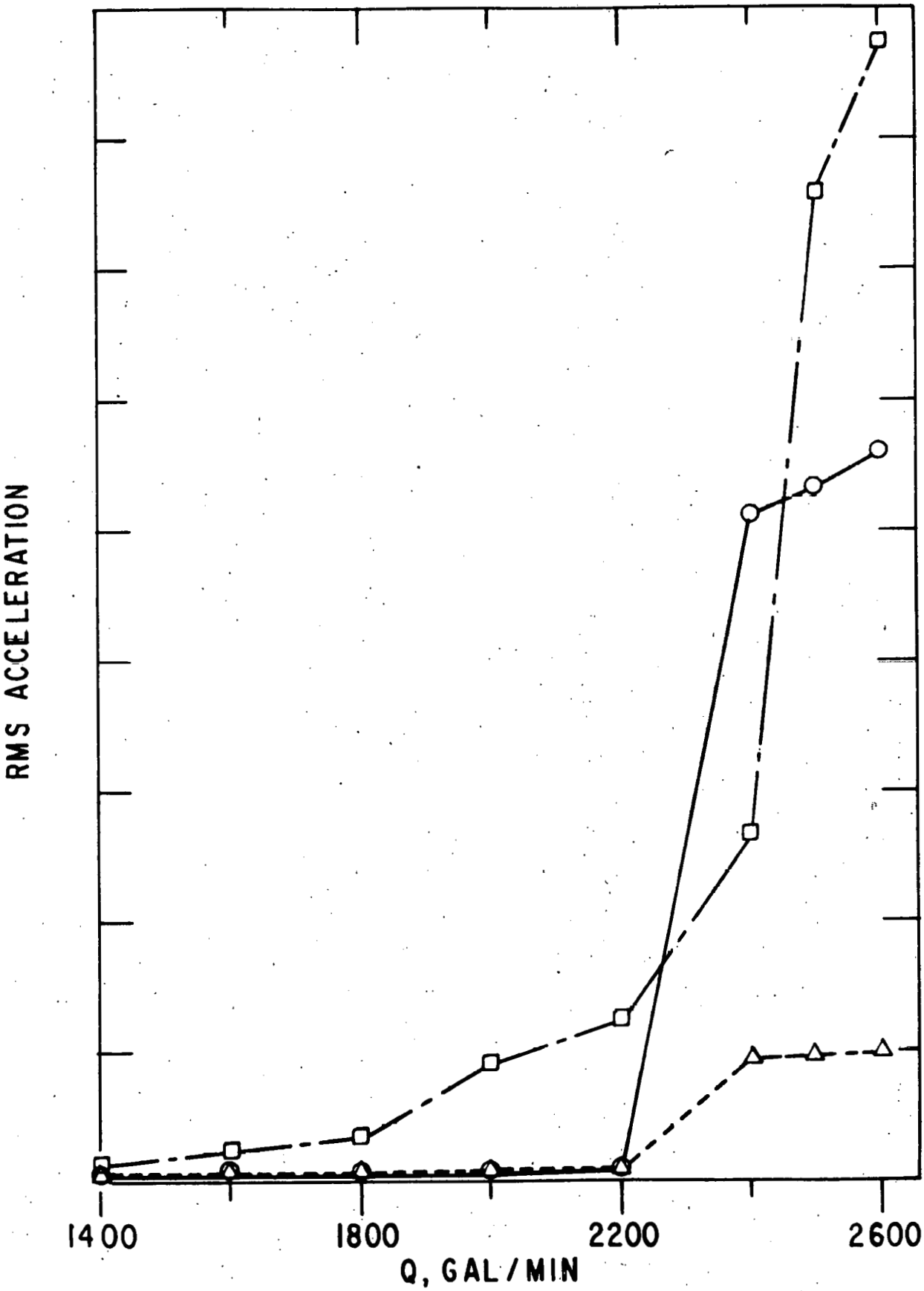

Fig. 17. RMS acceleration versus flowrate; Tube U-23 (Δ), Tube V-24 (○), Tube C-15 (□)

observations and response data cannot be explained by arguing that the instability was not audible as a result of the amplitudes being insufficient to cause impacting.

CASE 10

Case 10 is a 5-baffle, 6-crosspass configuration with 10 in. diameter inlet/outlet nozzles and a pass lane in the far window region (11 tubes removed), as illustrated in Fig. 8b. Again, the basic tube bundle was not "disturbed" from Case 7. That is, the stainless steel row U tubes were removed, Admiralty brass tubes were inserted, and the pass lane tubes pulled and tubesheets plugged without removing the bundle from the exchanger.

From the sensory observations (Appendix - Case 10) there was no doubt that the pass lane in the far window region had a significant effect on the dynamic behavior of the bundle. In particular, the instability threshold was not well defined in the sense that the very violent tube motion associated with loud, sustained impacting/rattling noise was never achieved. The lowest critical flowrate, with instability initiating in the far window region, was determined to be 2600 gpm. At a flowrate of 2700 gpm there was general large amplitude vibration in the far window region. Upon decreasing the flow, the instability dropped out in the range of 2400 to 2200 gpm. As a general observation, asymmetry was noted in comparing tube motion at the "top" and "bottom" of the far window region. For example, at 2600 gpm, while increasing the flow, the tubes at the bottom were experiencing large amplitude motion while tubes at the top showed little activity. With decreasing flow, at 2400 gpm the large amplitude motion at the bottom had ceased, while the tubes at the top were still vibrating with large amplitude.

Accelerometers were installed in tubes U-5, 19, and 21, and tube V-20 and analyzed "on line" for a range of flowrates. Curves of rms acceleration versus flowrate are given in Fig. 18. Tubes U-19, U-21, and V-20 were selected to be instrumented as they are adjacent tubes in a triangular pattern (see Fig. 8b). It is interesting to note that the response of tube U-19 (Fig. 18a) is approximately an order of magnitude less than that of its neighbors, U-21 (Fig. 18b) and V-20 (Fig. 18c). From Figs. 18b and 18c one would conclude that the critical flowrate is in the range 2600 to 2650 gpm; Fig. 18d indicates that tube U-5 goes unstable at a higher flowrate;

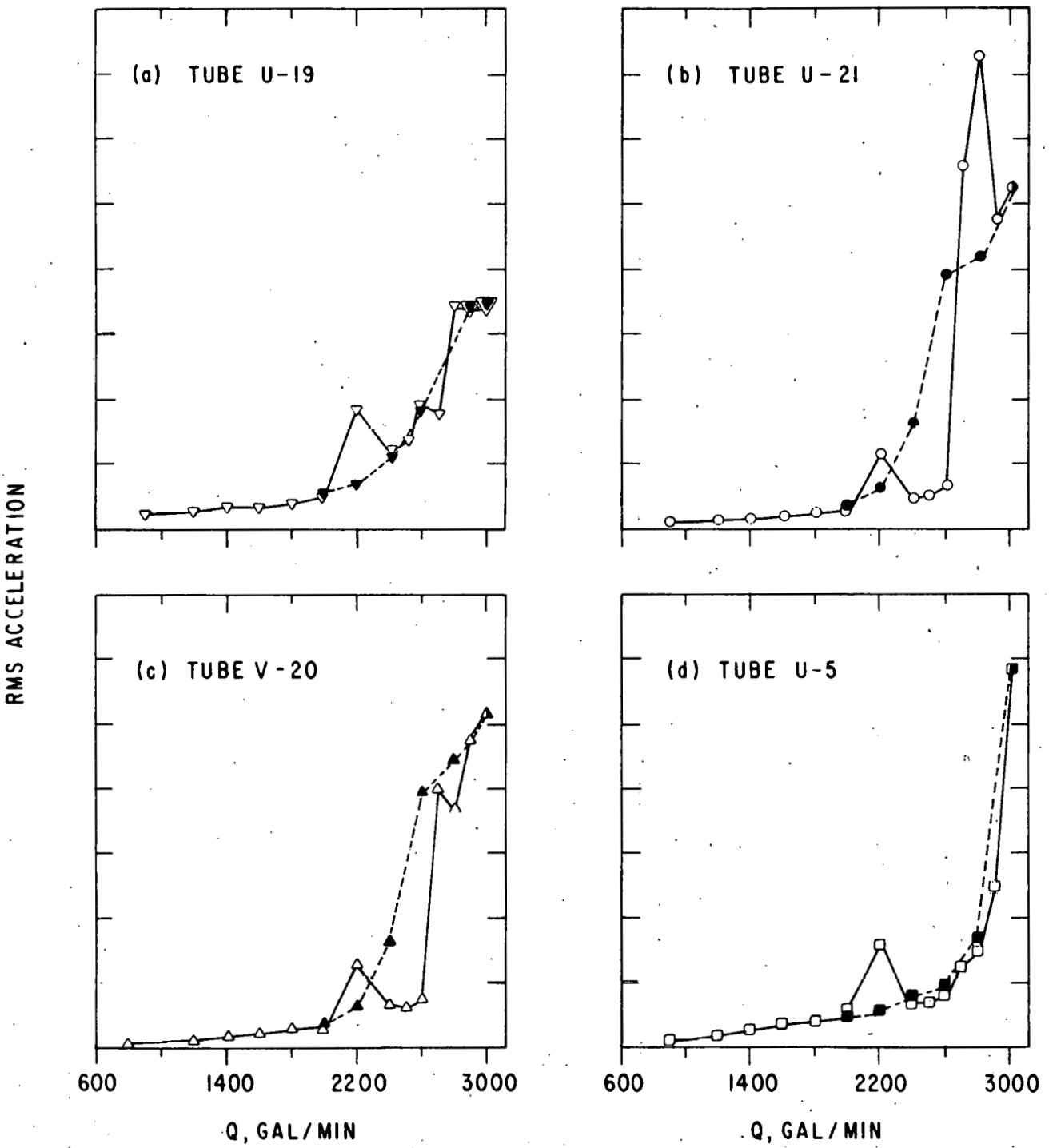

Fig. 18. RMS acceleration versus flowrate; (a) Tube U-19 (▽), (b) Tube U-21 (○), (c) Tube V-20 (△), (d) Tube U-5 (□); Open symbol - increasing flow, solid symbol - decreasing flow

and Figs. 18b and 18c show a hysteresis effect that has tubes U-21 and V-20 dropping out of instability at a flowrate of approximately 2300 gpm. These three results all agree with the results from sensory observations as discussed above and presented in Table 8.

In Fig. 19, frequency response curves from tube V-20 are given for increasing and decreasing flowrates. Response spectra for flowrates from 900 to 2600 are representative of turbulent buffeting excitation. The sharp, single-frequency response at 2700 gpm indicates that the transition from turbulent buffeting to fluidelastic instability took place in the range 2600 to 2700 gpm; the instability mode frequency is 22.2 Hz. The multiple frequency response at flowrates from 2800 to 3000 gpm is expected to be the result of impacting with adjacent tubes and/or rattling in the baffles. As the flowrate is decreased from 3000 gpm it is interesting to observe that a well-defined, single-frequency instability mode frequency appears once again. The dropout of instability, or transition from instability to a dominant turbulence response occurs between 2200 and 2000 gpm as indicated by the change in character of the response spectra. Again, these results are in good agreement with the results from sensory obervations.

CASE 11

Case 11 is a 5-baffle, 6-crosspass, full-tube bundle configuration and is a repeat of Case 7. The "history" of the bundle is as follows: Without removing the tube bundle from the shell (1) Row U was removed (Case 8); (2) Row U was replaced with stainless steel tubes (Case 9); (3) Row U tubes were removed and replaced with original, Admiralty brass tubes and a pass lane created by removing 11 tubes in far window region on centerline through nozzles (Case 10); the pass lane was filled with brass tubes to return to a full bundle configuration (Case 11).

From sensory observations (Appendix - Case 11), the threshold flowrate for the onset of instability was determined to be 2140 gpm. At a flowrate of 2400 gpm general large amplitude vibration was occurring in the far window region. Upon decreasing the flow, fluidelastic instability was observed to drop out at 1700 gpm. The instability threshold was somewhat higher than the previous full bundle test result of 1970 gpm (Case 7). Additionally, the instability did not seem to be as "violent."

Acceleration-time signals from accelerometers located in tubes U-5, 19, 21 and V-20 were recorded and analyzed. In Fig. 20, rms acceleration

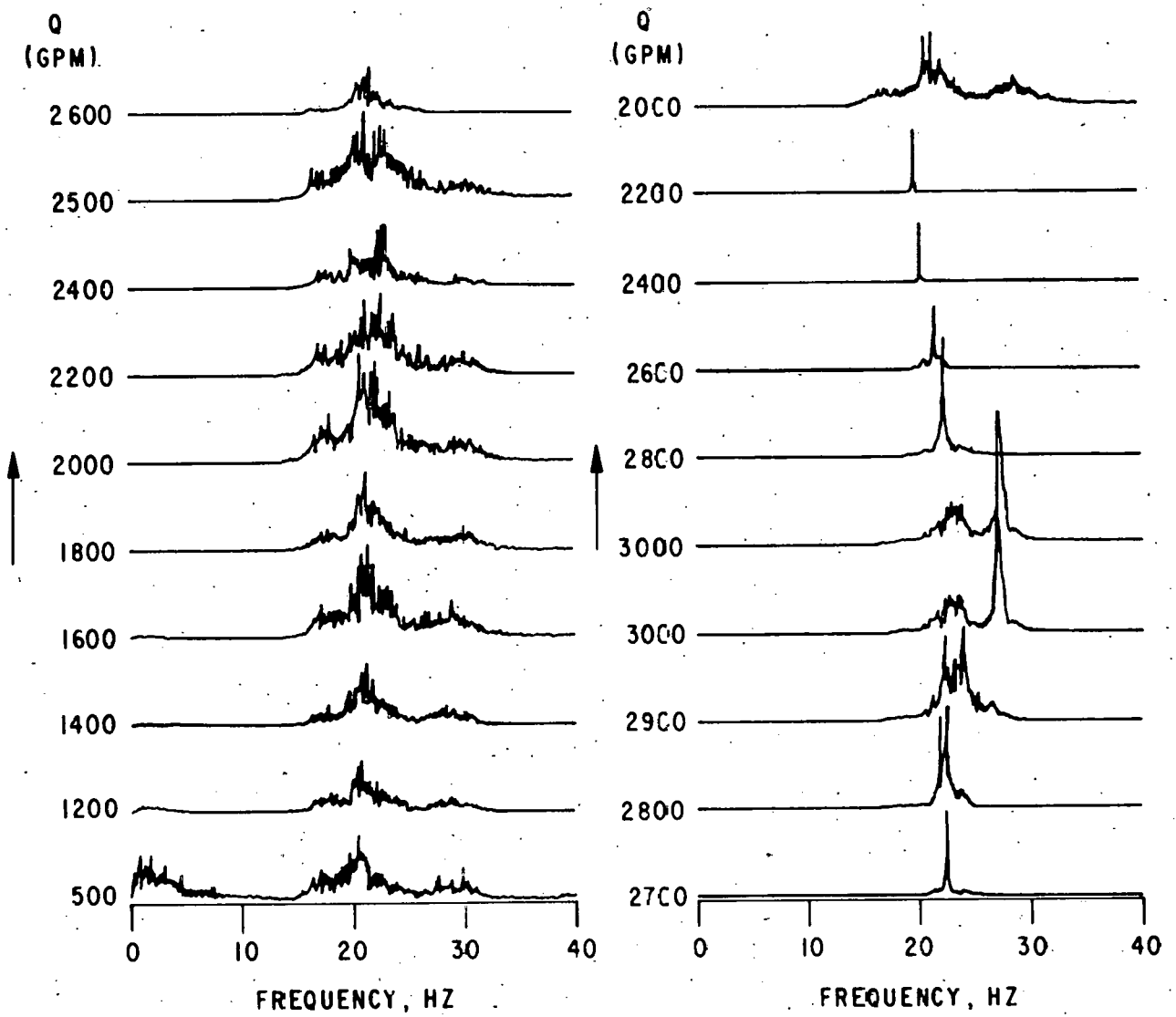

Fig. 19. Frequency response curves; Tube V-20

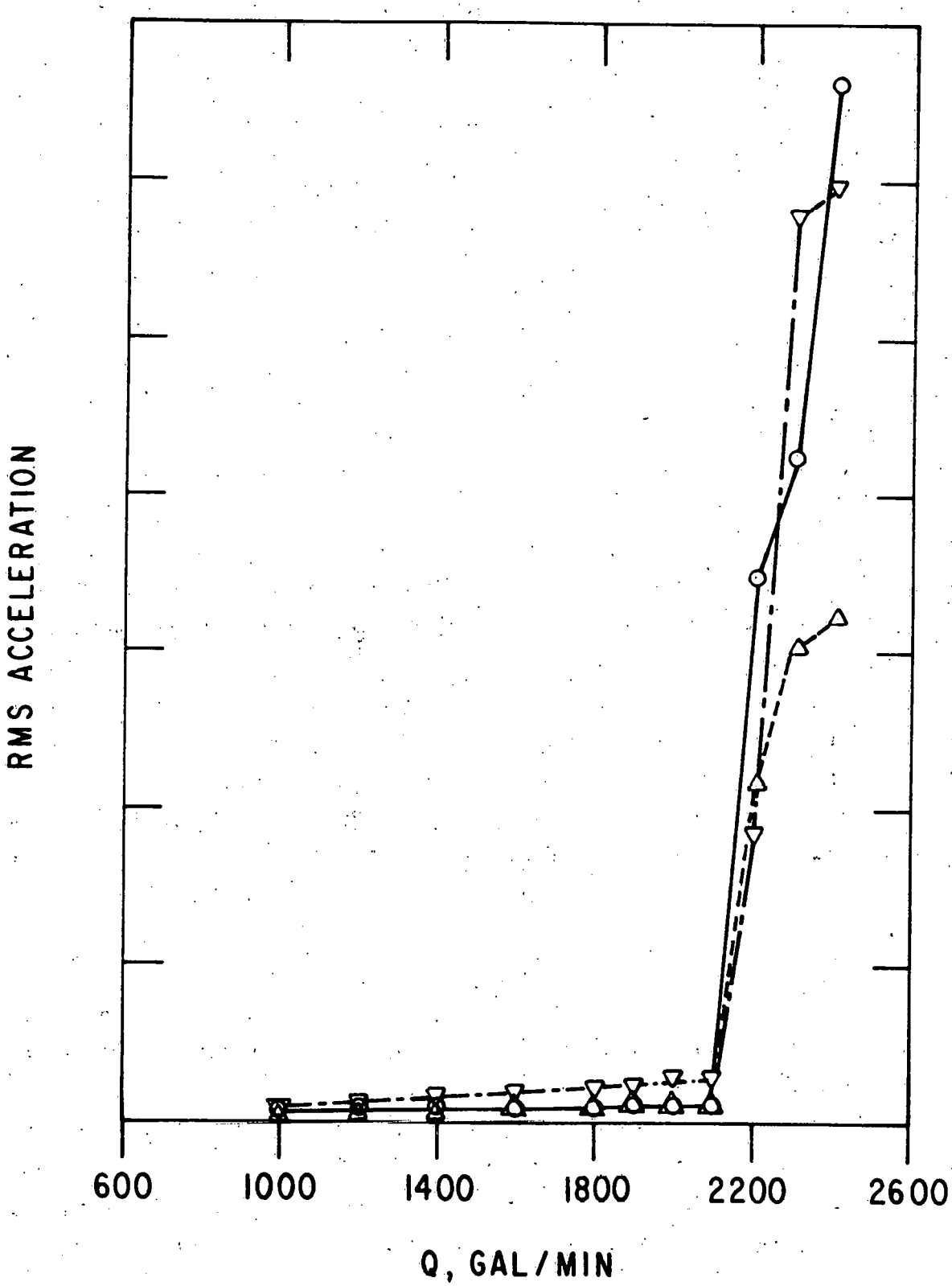

Fig. 20. RMS acceleration versus flowrate; Tube U-21, (O), Tube V-20 (Δ), Tube U-5 (∇)

is plotted as a function of flowrate for tubes U-5, U-21, and V-20. From Fig. 20, one would conclude that instability occurs in the flowrate range 2100 to 2200 gpm. This is in agreement with the values of 2140 gpm determined from sensory observations.

CASE 12

Case 12 is a 5-baffle, 6-crosspass configuration with 10 in. diameter inlet/outlet nozzles and pass lanes in both the near and far window regions (22 tubes removed), as illustrated in Fig. 8c. The basic bundle was not disturbed from Case 7.

Based on sensory observations (Appendix - Case 12), the critical flowrate was determined to be 2870 gpm. By the time a flowrate of 3050 gpm was reached, general large amplitude vibration could be observed in the far window region. Audible impacting/rattling ceased at a flowrate of 2500 gpm; this was identified as the flowrate for dropout of instability. As in Case 10, asymmetry was observed with tubes at the top of the far window region first vibrating at amplitudes sufficiently large to be visible (1800-2400 gpm); then tubes at the bottom of the region vibrating more strongly (~2600 gpm); next, row U vibrating from center to bottom (3000 gpm); finally, general large amplitude motion in far window region (3100 gpm).

As in previous test cases, tubes U-5, -19, -21, and V-20 were instrumented with accelerometers. In Fig. 21, rms acceleration is plotted as a function of flowrate. The abrupt increase in acceleration response as the flowrate is increased to 3000 gpm from 2800 gpm indicates that the critical flowrate falls within this range. This result agrees with the determination, from sensory observations, of 2870 gpm as the critical flowrate.

CASE 13

Case 13 is a 5-baffle, 6-crosspass configuration with 10 in. diameter inlet/outlet nozzles and the tubes in the two "window regions" removed to give a no-tubes-in-window (NTIW) configuration; see Fig. 8d.

The flowrate was increased from 1600 to 4590 gpm and sensory observations of tube bundle response made (Appendix - Case 13). No significant tube vibration occurred over the range of flowrates tested. However, the tie bars were observed to experience large amplitudes that increased with

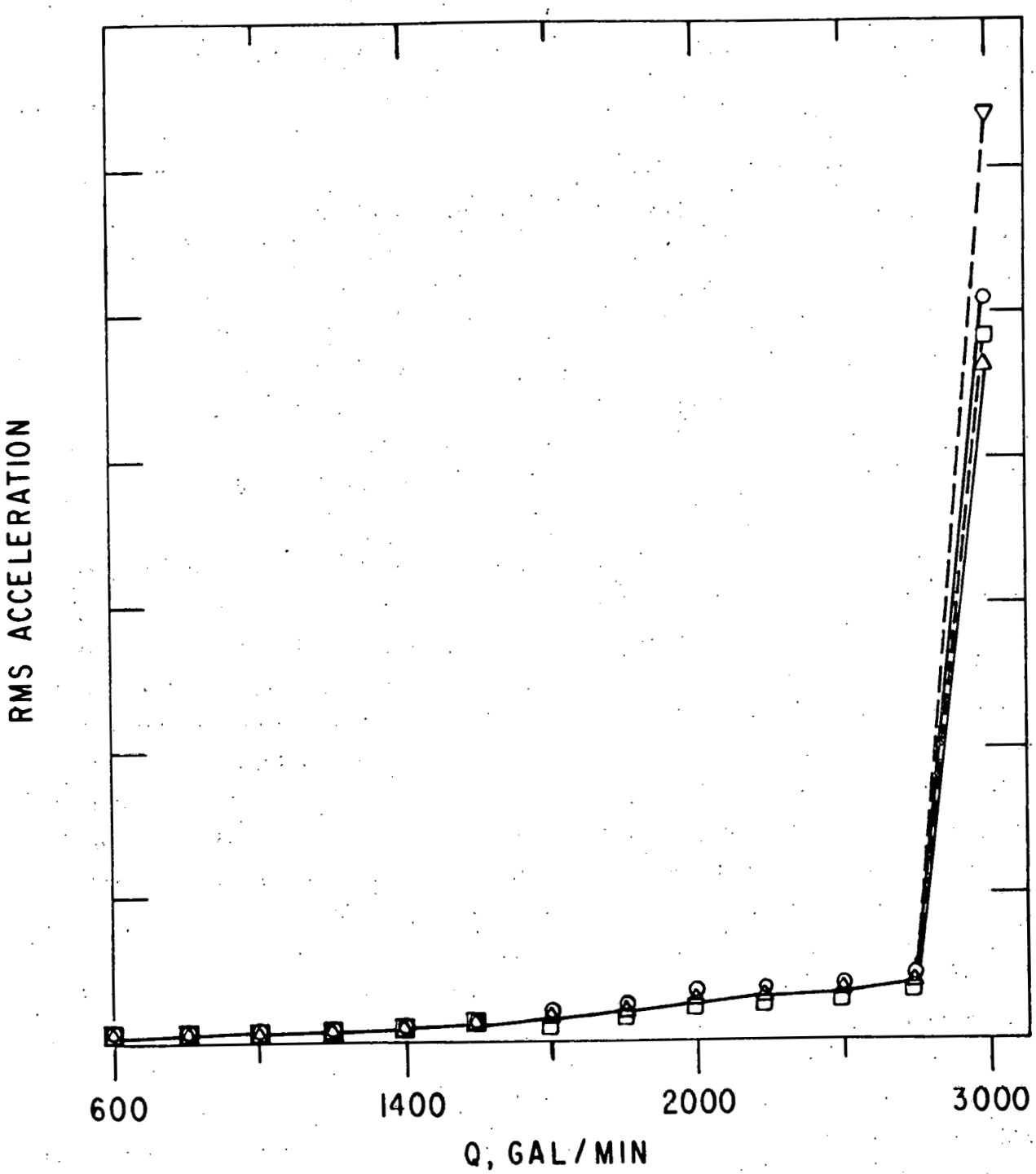

Fig. 21. RMS acceleration versus flowrate; Tube U-5 (O), Tube U-19 (Δ), Tube U-21 (∇), Tube V-20 (□)

flowrate. Rattling of the tie bars was readily audible. No tube vibration response measurements were made.

CASE 14

Case 14 is a finned tube bundle in a 5-baffle, 6-crosspass configuration with 10-in. diameter inlet/outlet nozzles and the tubes in both window regions removed to give the so-called NTIW configuration; see, again, Fig. 8d.

The flowrate was incrementally increased from 1000 to 6000 gpm and sensory observations of tube bundle response made (Appendix - Case 14). At high flowrates (>4000 gpm), virtually all of the tubes in the bundle experienced a general low level vibration. However, large amplitude tube vibration, as would be indicative of fluidelastic instability, was not observed. As in the NTIW test with smooth tubes (Case 13), the tie bars in the window regions vibrated with relatively large amplitudes, sufficient to cause them to impact with the shell wall. No tube vibration response measurements were made since an instability was not observed.

CASE 15

Case 15 is a full bundle of finned tubes in a 5-baffle, 6-crosspass configuration with 10 in. inlet/outlet nozzles.

The finned tube bundle of this test case responded significantly different from the corresponding smooth tube bundles that were previously tested and reported. In particular, it was not possible to identify a well-defined critical flowrate from sensory observations (Appendix - Case 15). The observations that were made can be summarized as follows: Large amplitude motion occurred first at the bottom of the far window region (~2400 gpm); tubes at the bottom of the near window region experienced large motion before row U tubes and tubes at top of the far window region - the loudest (in fact, only) impacting noise came from this region (>3200 gpm); tubes in the middle of row U did not vibrate until a high flowrate (4100 gpm) was reached, and the vibration was not violent.

For one test run, the following tubes, all located at the "bottom" of the far window region, were instrumented with accelerometers: V-38, -40, -42; W-37, -39, -41; X-36, -38; and Y-37. A second test run was performed with these tubes instrumented: F-8, -40; G-9, -39; U-9, -25, -39; and V-8, -24. In Figs. 22-25, rms vibration response is plotted as a function of flowrate for select tubes in various regions of the tube bundle. Results

deduced from the dynamic behavior of the tubes, as indicated by these rms response curves, can be compared with sensory observations of tube bundle behavior as summarized above and documented in the Appendix.

RMS displacement response data from tubes V-40, V-42, and W-41 are given in Fig. 22. These three tubes are adjacent tubes on a triangular layout and are located at the "bottom" of the far window region (see Fig. 7). A rather abrupt increase in response occurs at a flowrate of ~2200 gpm. This agrees with visual observations. As flowrate is increased further ($Q > 2400$ gpm) the response tends to drop off or remain nearly the same with little further increase. This could be the result of impacting, with adjacent tubes limiting tube motion. However, no audible impacting/rattling noise was detected (Appendix - Case 15).

In Fig. 23, rms acceleration data are plotted as a function of flowrate for two pairs of tubes located in the near window region. One pair (tubes F-8 and G-9) are located at the "top" of the window region; the second pair (tubes G-39 and F-40) are located at the "bottom." Visual/aural observations (Appendix - Case 15) yielded the following results: At 3200 gpm, "can hear rattling/impacting noise from bottom of near window region;" at 3600 gpm, "impacting noise level from near window tubes has increased." Fig. 23 shows the response of tube F-40 to increase in the flow range 3000 to 3400 gpm and to peak at 3600 gpm; a behavior that, again, agrees with observation. While the motion of the adjacent tube, G-39, does not follow that of tube F-40, this should not be of concern since Chen[3,4] has shown that coupling with adjacent tubes is not necessary when fluid-damping controlled instability is the dominant instability mechanism.

Sensory observations at a flowrate of 3400 gpm showed tube motion at the top portion of the window regions, with tube motion greater in the far window, and no observable motion of tubes in center of row U. In fact, there was no observable motion of the middle of row U at 3900 gpm and it wasn't until a flowrate of 4100 gpm that all of row U vibrated with appreciable amplitude. In Figs. 24 and 25, rms acceleration data are plotted versus flowrate for pairs of tubes located at the top of the far window (tubes U-9 and V-8, Fig. 24) and in the middle of rows U and V (tubes U-25 and V-24, Fig. 25). It can be seen from these figures, that

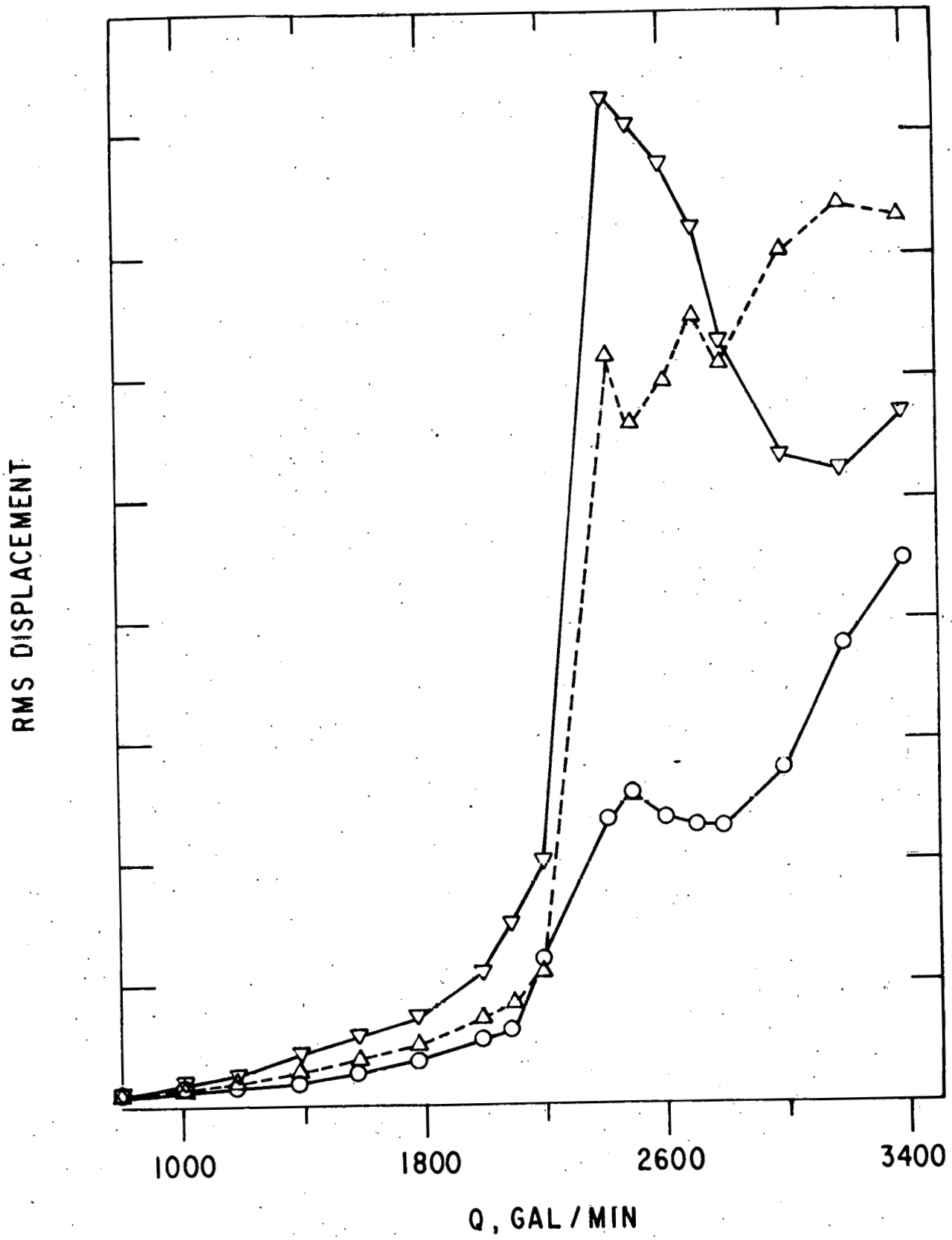

Fig. 22. RMS displacement versus flowrate; Tube V-40 (O), Tube V-42 (Δ), Tube W-41 (∇)

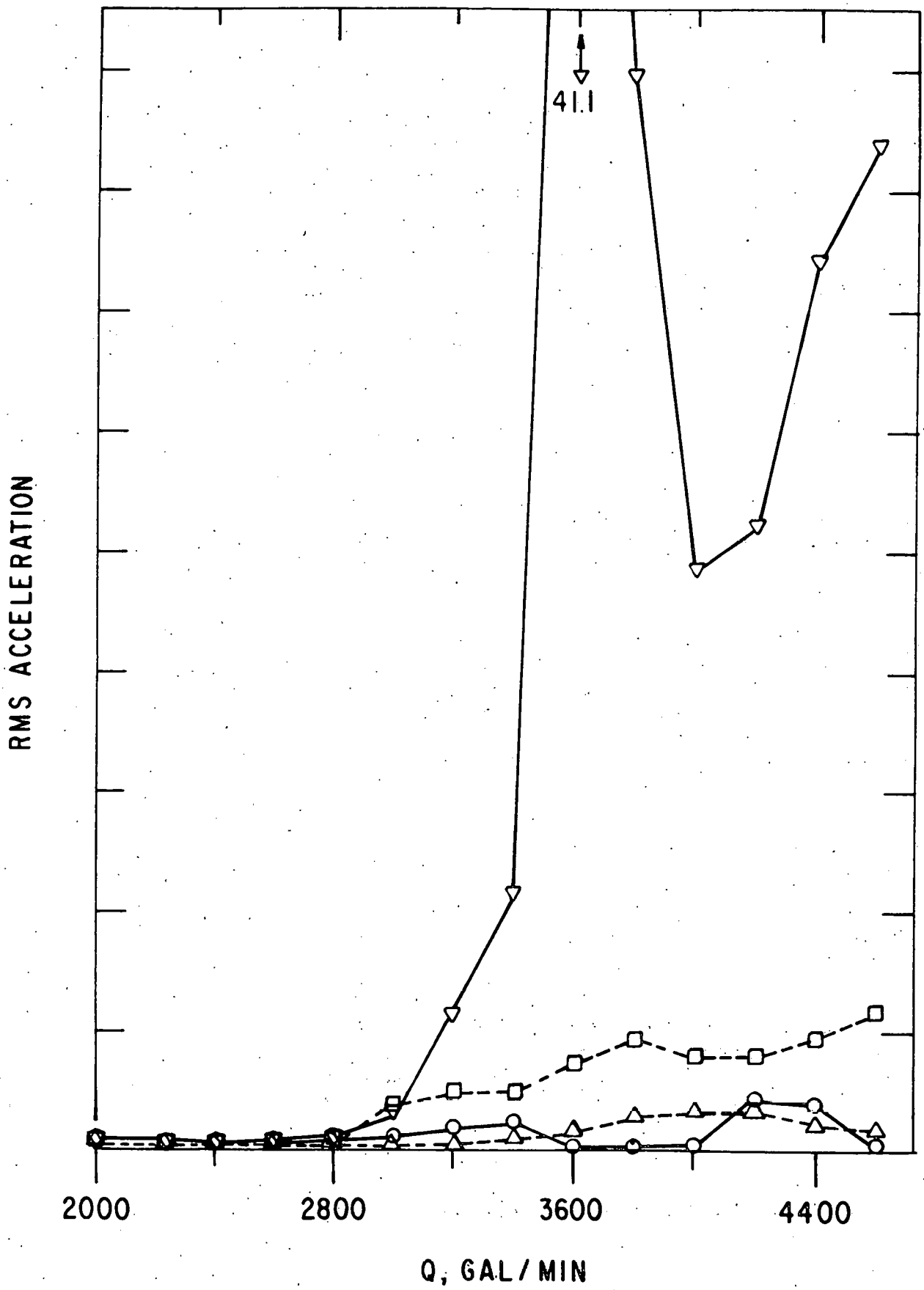

Fig. 23. RMS acceleration versus flowrate; Tube F-8 (O), Tube G-9 (Δ), Tube F-40 (V), Tube G-39 (□)

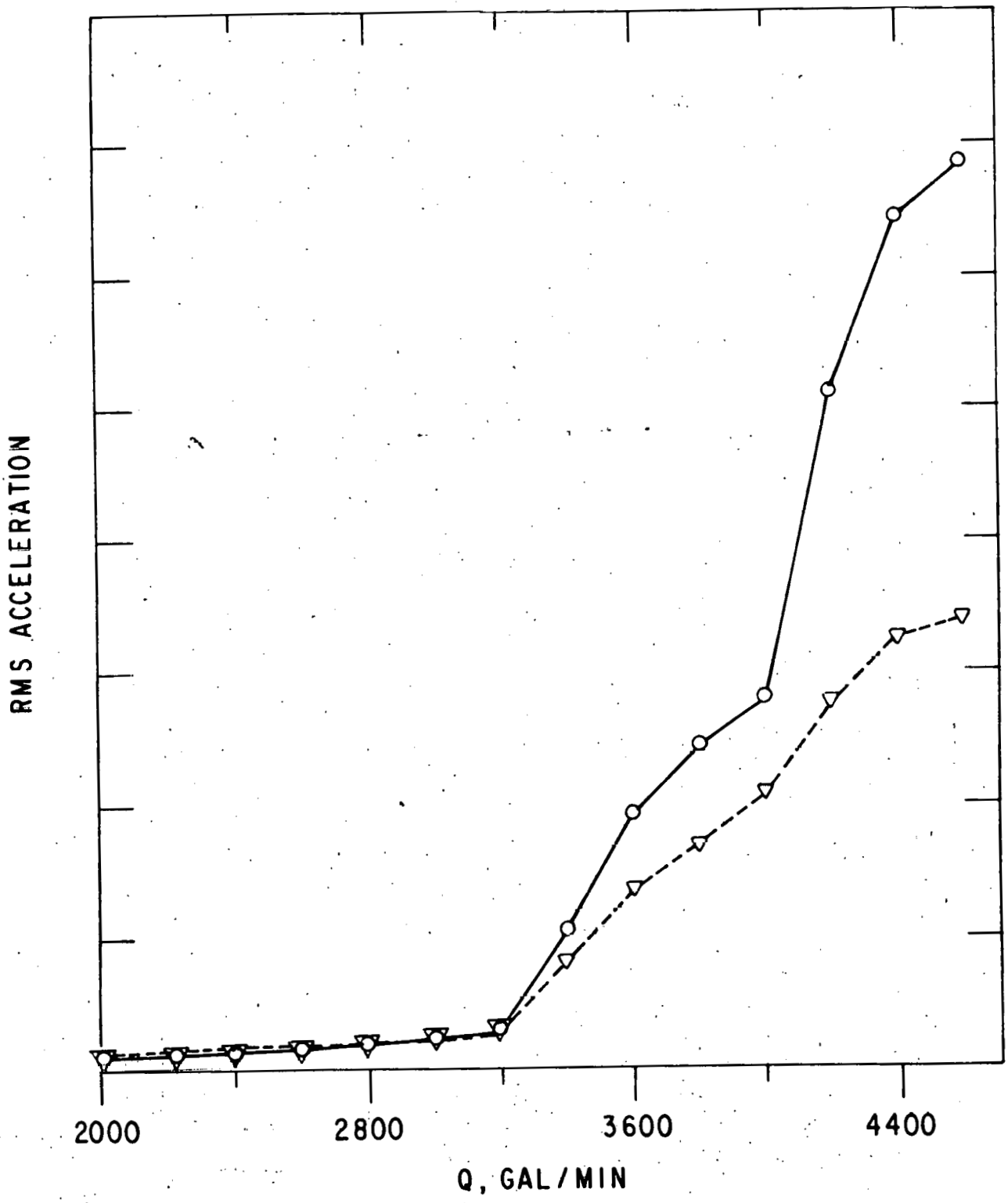

Fig. 24. RMS acceleration versus flowrate; Tube U-9 (O), Tube V-8 (∇)

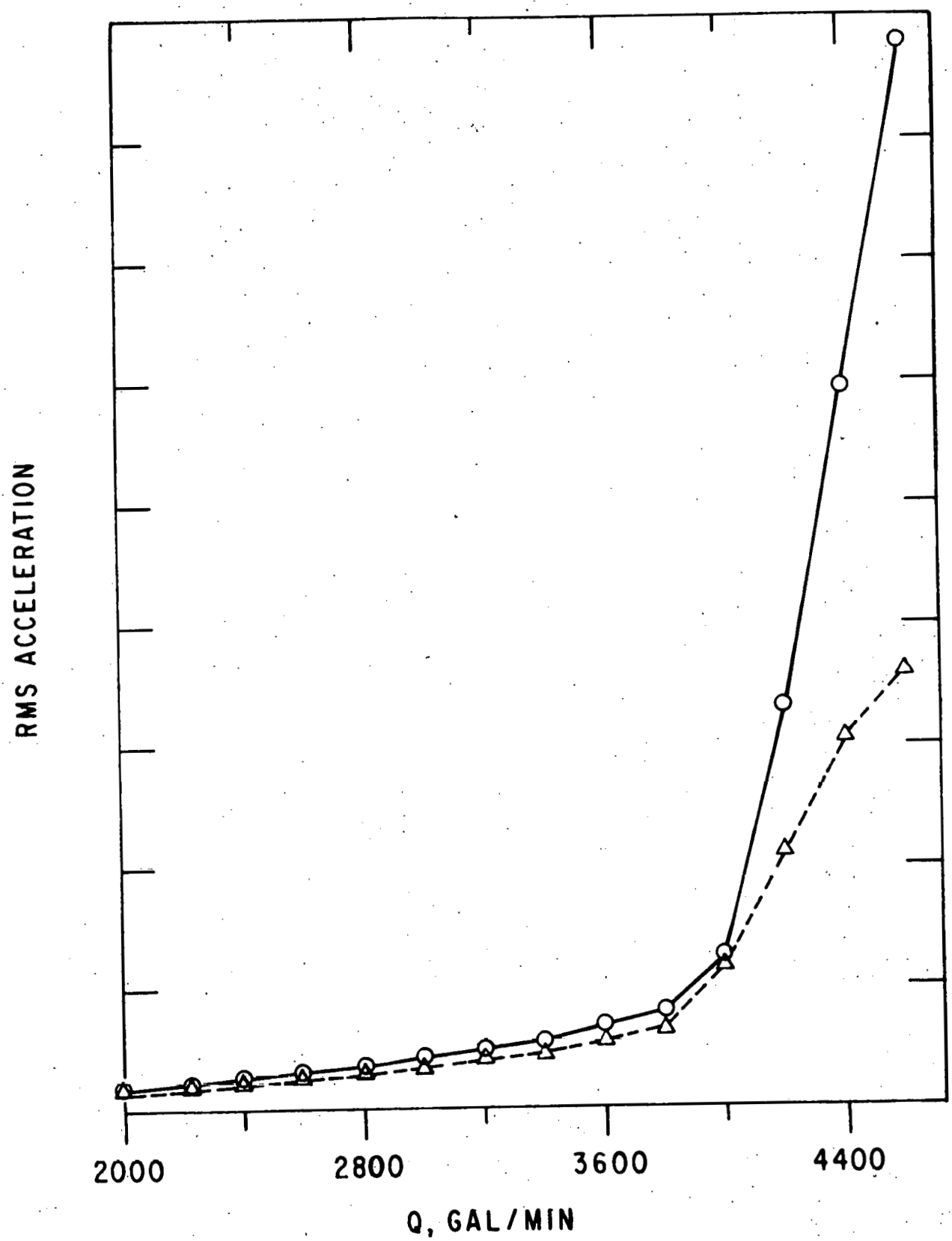

Fig. 25. RMS acceleration versus flowrate; Tube U-25 (O), Tube V-24 (Δ)

the tube behavior indicated by the acceleration response curves agrees with results from observation.

Extensive data reduction was carried out to obtain frequency spectral density representations of the acceleration-time histories. Typical results are presented in Figs. 26 and 27 for a 3-span, far window region tube (V-40) and a 4-span, near window region tube (F-40), respectively. The dynamic behavior is similar to that shown in Figs. 15 and 19 in the sense that at subcritical flowrates the response is over a broad band of frequencies and when the instability flowrate is reached the tube responds in a well-defined single frequency instability mode.

From Fig. 26 it can be concluded that the transition to instability occurs between the flowrates of 2000 and 2200 gpm; this agrees with sensory observations. It is interesting to note that at flowrates above the critical (>2200 gpm), the single-frequency response is maintained. This would indicate that the instability amplitudes are moderate and do not result in tube-to-tube impacting, as impacting would be expected to excite additional frequencies as in Fig. 19. This result also agrees with sensory observation of "no audible impacting/rattling"; see Appendix - Case 15.

The frequency response spectra in Fig. 27 are from the 4-span, near window tube, F-40. Typically, the near window tubes have been observed to respond at a higher frequency than the far window, 3-span tubes. This tendency to respond at higher frequencies is shown by the spectra corresponding to flowrates of 2000, 2400, and 2800 gpm in Fig. 27; response at frequencies centered about a frequency of 75 Hz is indicated in addition to lower frequency response band excitation. At a flowrate of 3200 gpm an instability at an instability mode frequency of 67.4 Hz is indicated by the sharp, single-frequency response spike; sensory observations (Appendix - Case 15) report audible rattling/impacting from the bottom of the near window region at this flowrate. As the flowrate is increased further, from 3200 to 3600 gpm, the instability mode seems to shift from 67.5 Hz (at 3200 gpm) to 21.5 Hz (at 3400 gpm) to 11.4 Hz (at 3600 gpm); it apparently "locks in" at 11.4 Hz. Sensory observations report an increase in impacting noise at 3600 gpm and the rms acceleration versus flowrate curve (Fig. 23) peaks at this value of flowrate.

Space limitations preclude the inclusion of the complete set of frequency response spectra obtained from the instrumented tubes. However,

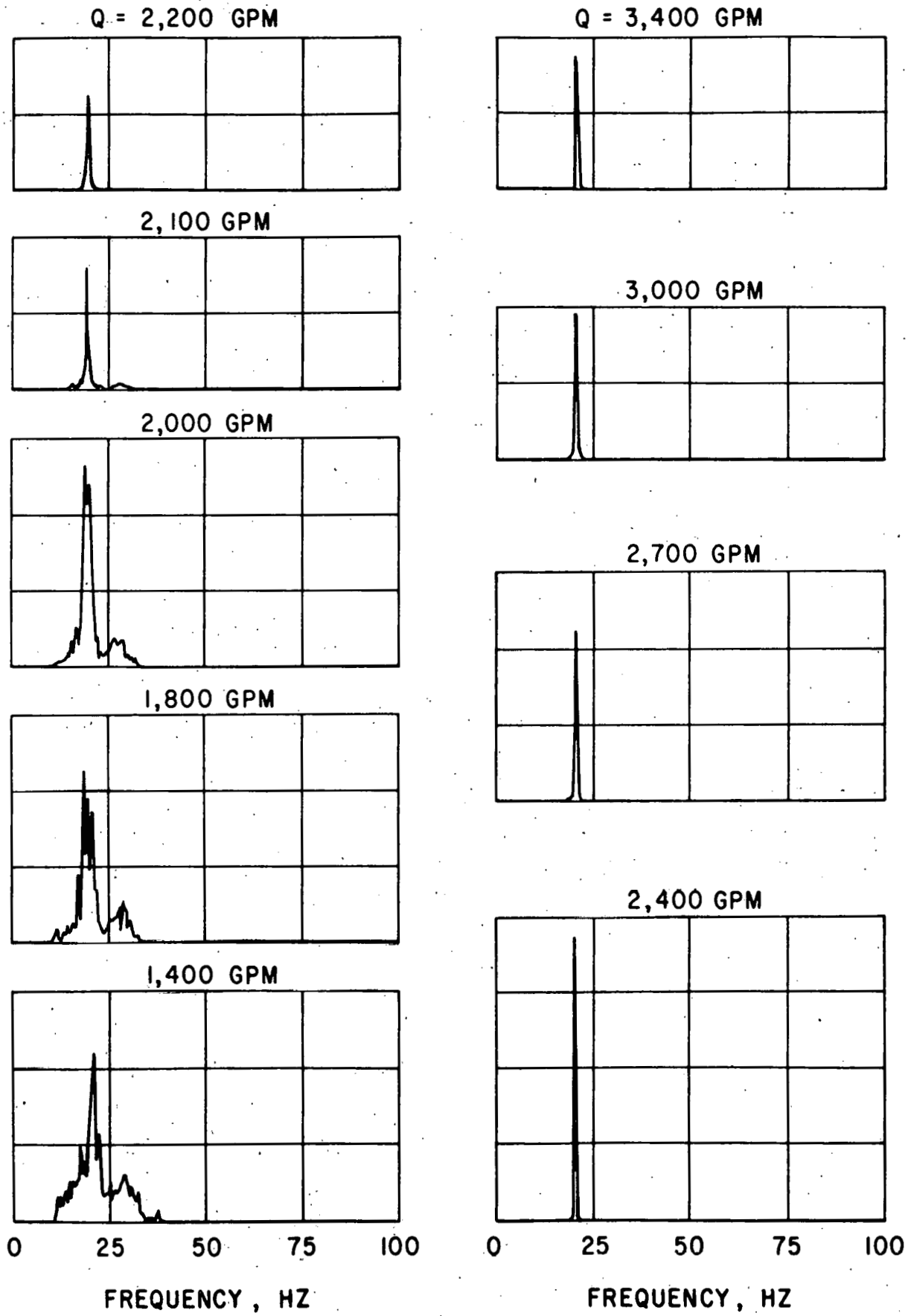

Fig. 26. Frequency response spectra; Case 15 - Tube V-40

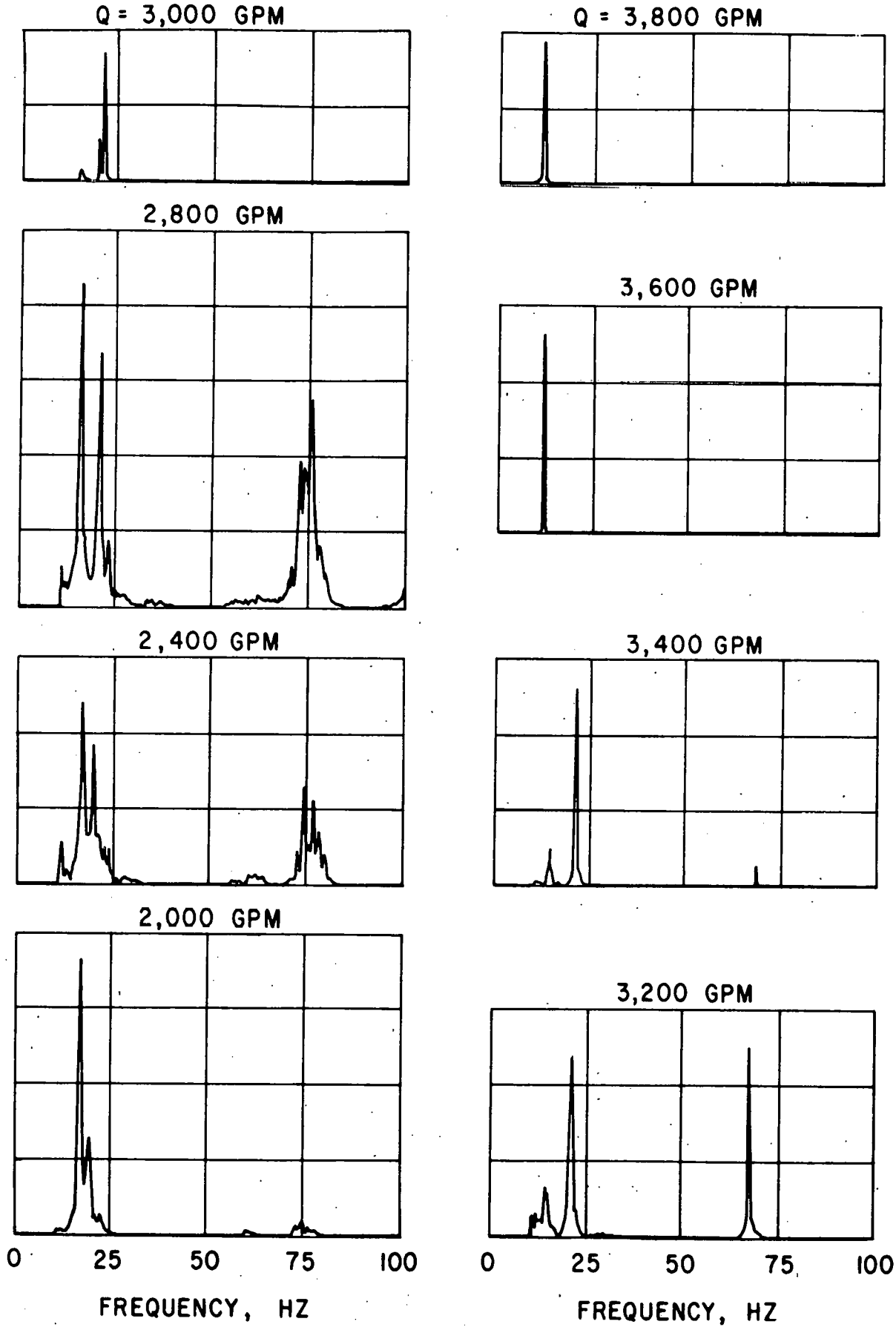

Fig. 27. Frequency response spectra; Case 15 - Tube F-40

it should be noted that from an analysis of the frequency response spectra alone, it is possible to deduce the dynamic behavior of the tube bundle. This is illustrated in Fig. 28 where the critical flowrates for individual tubes, as determined from analysis of the frequency spectra, are identified.

B. Pressure Drop

Pressure drop measurements were made during flow testing for all of the tube bundle configurations tested. A schematic showing the locations of the pressure taps is given in Fig. 9. Overall (inlet/outlet) pressure drop is measured between taps designated A and I on Fig. 9. When inlet-to-outlet pressure drop is plotted as a function of flowrate on log-log paper the data can be correlated with a straight line. This implies that the overall pressure drop can be related to flowrate by a power function relationship of the form

$$\Delta p = \beta Q^{\alpha} \qquad (12)$$

where β and α are constants for a particular tube bundle configuration.

In Table 10, values for the constants in Eq. (12) are listed. The exponent α is seen to vary from 1.80 to 1.92. To allow for easy comparison of the different tube bundle configurations, the overall pressure drop at a flowrate of 2000 gpm is also listed. It is of interest to note that with 14 in. inlet/outlet nozzles the pressure drop (11.9 psi) is significantly less than that with 10 in. nozzles (14.9 psi). As expected, with pass lanes the pressure drop is reduced from what it is with a full tube bundle. Pressure drop with a full bundle of finned tubes (15.3 psi) is slightly greater than that for a full bundle of smooth tubes (14.9 psi). However, for the NTIW configuration the pressure drop with finned tubes (4.7 psi) is less than that with smooth tubes (5.2 psi).

In Fig. 29 the normalized fractional distributions of the pressure drop are given for each of the tube bundle configurations. The overall pressure drop is set equal to unity and the fractional drops are calculated for each flowrate tested and then averaged to obtain the results given in Fig. 29.

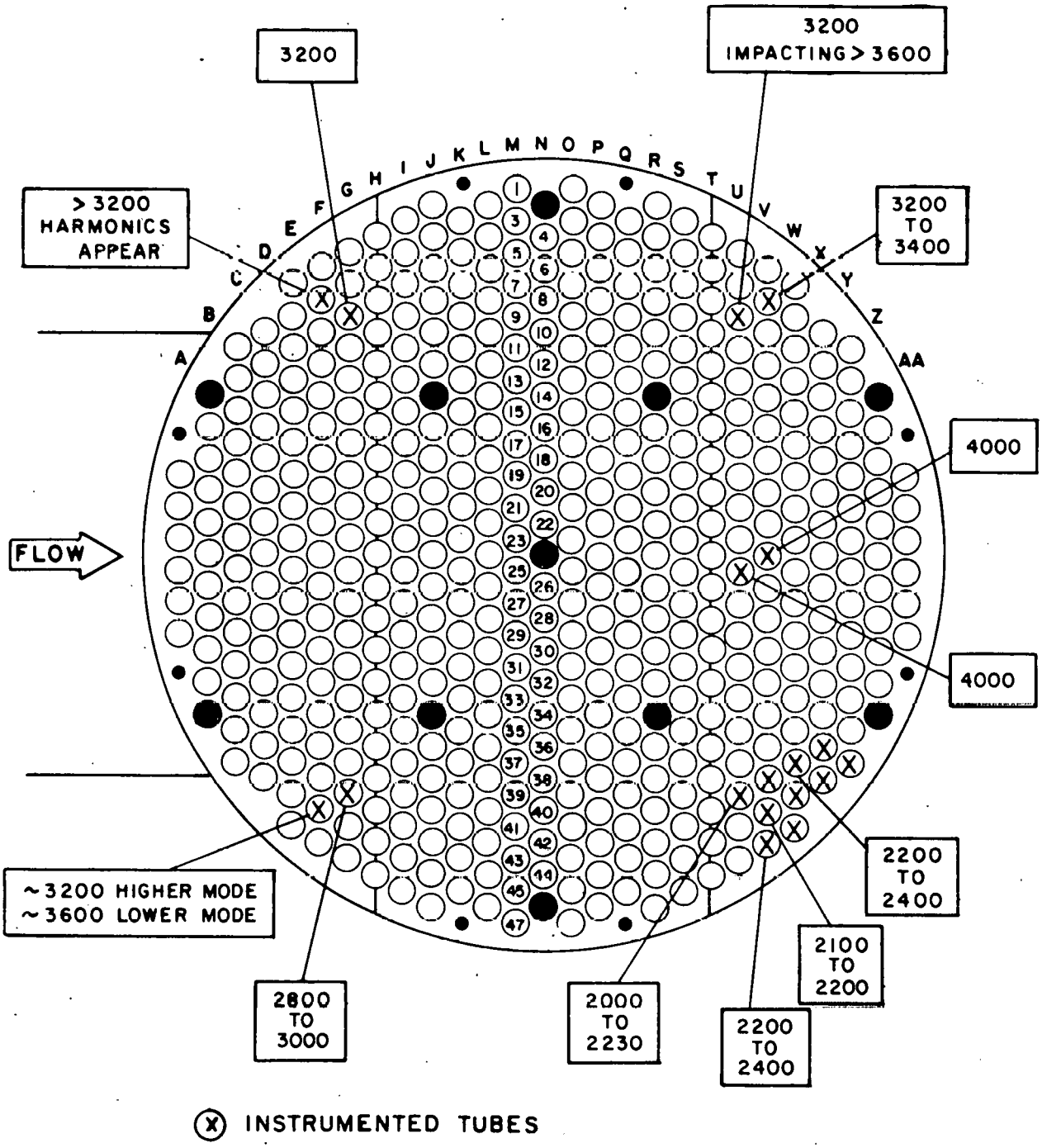

Fig. 28. Map of critical flowrates determined from analysis of frequency response spectra

Table 10. Overall (inlet/outlet) pressure drop

Test Case	Tube Bundle Configuration	$\Delta p\|_{Q=2000\ gpm}$ (psi)	Eq. (12) constants*	
			α	$\beta \times 10^6$
6	Full - 14 in. nozzles	11.9	1.90	6.36
7	Full - 10 in. nozzles	14.9	1.88	9.27
8	Row U removed	11.1	1.87	7.52
9	Row U stiffened	14.3	1.92	6.55
10	Pass lane - far window	12.4	1.91	6.16
11	Full - 10 in. nozzles	-	-	-
12	Pass lane - both windows	8.9	1.91	4.41
13	NTIW	5.2	1.80	5.97
14	NTIW - finned tubes	4.7	1.90	2.53
15	Full - finned tubes	15.3	1.91	7.48

* $\Delta p = \beta Q^{\alpha}$, where $\Delta p \sim$ psi, $Q \sim$ gpm

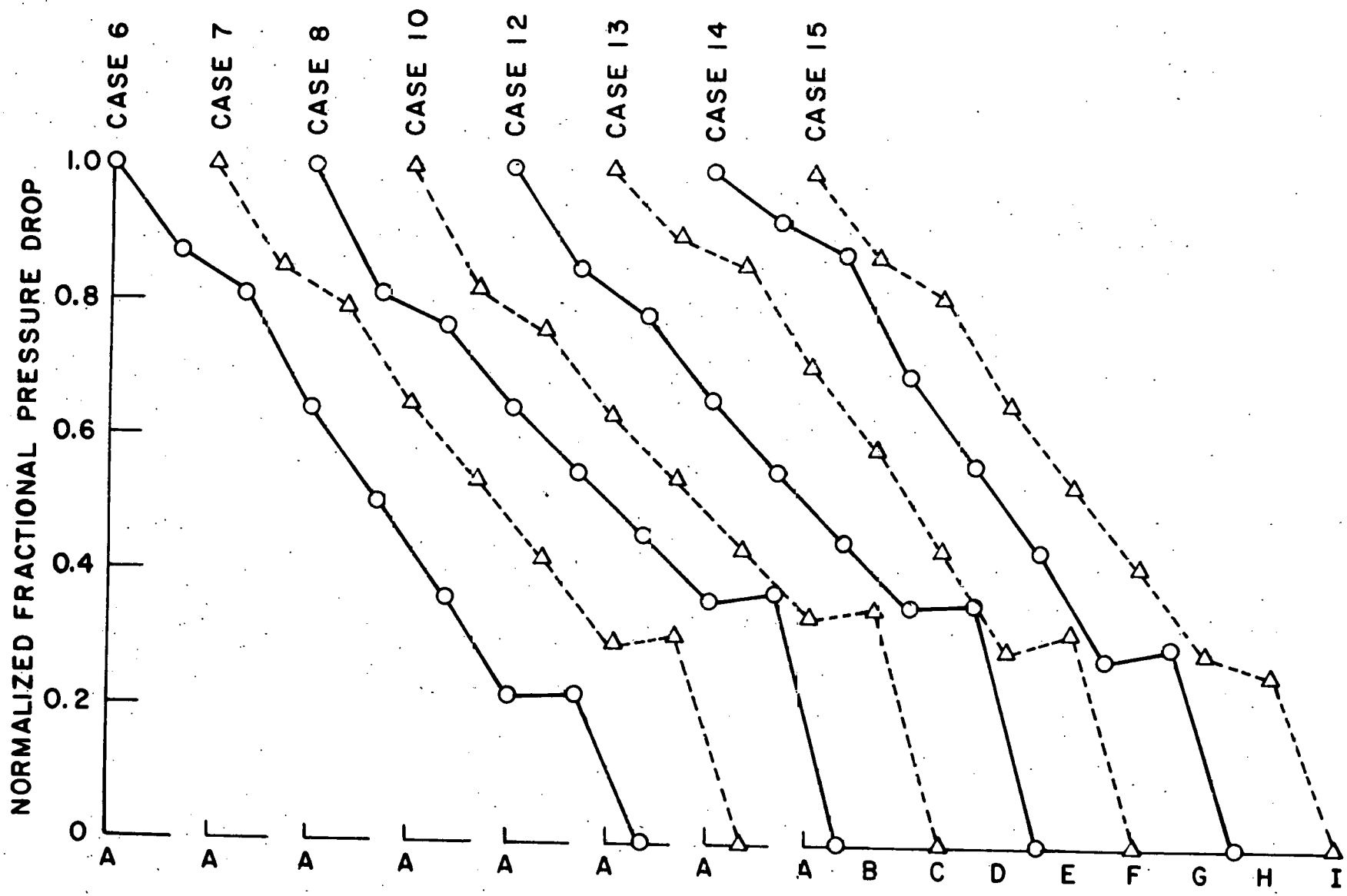

Fig. 29. Fractional distribution of pressure drop averaged and normalized to total pressure drop; See Fig. 9 for location of pressure taps

VI. CONCLUDING REMARKS

Nine different tube bundles, in a basic 5-baffle, 6-crosspass configuration on a 30°-triangular layout with P/d ratio equal to 1.25, have been flow tested for vibration and are reported herein. The testing focused on identification of the lowest critical flowrate for instability. Nevertheless, pressure drop information was also generated, along with data relating to the subcritical vibration of the tubes.

At subcritical flowrates, turbulent buffeting dominates. This broad-band force generally excites a large number of coupled modes in the first frequency band of a given tube as illustrated in the frequency response presentations of the data (see Figs. 15, 16, 19, 26 and 27). Lower and upper bounds on the first frequency band have been computed and are given in Eqs. (9)-(11) for 3-, 4-, and 6-span tubes, respectively. A comparison of calculated bounds with experimental results shows reasonably good agreement. For example, compare the calculated frequency band of 18.8 to 51.3 Hz for a 3-span tube (Eq. (9)) with the subcritical frequency response given in Fig. 15b. Also, the 4-span tube frequency response shown in Fig. 27 has frequency contributions over a relatively larger range in agreement with the frequency band range of 19.5 to 120.4 Hz given by Eq. (10). Test results have shown that flow further enhances the "spread" of the frequency band; see Fig. 15b, for example. Subcritical rms displacement at midspan of the tubes is typically small (<4 mils) and not expected to result in rapid tube failure. However, the effects of low level tube vibration on the reliability of heat exchangers designed for long lifetimes remains a concern.

With the exception of the NTIW bundles, all of the tube bundles tested experienced fluidelastic instability within the range of flowrates tested. Various criteria were applied to identify the critical flowrate associated with the onset of instability. For the subject tests, in which the tubes are open at the ends and it is possible to sight down the tube bores during flow testing, sensory observations are found to be generally reliable in identifying the onset of large amplitude tube vibration and associated impacting/rattling indicative of fluidelastic instability. However, the method is subjective and requires engineering judgment. The transition from a broad-band frequency response to a single frequency (instability mode) response is perhaps the most precise method. However,

this method requires selection and instrumentation of a particular tube as well as relatively sophisticated data processing. In general, these methods serve to complement one another and together can be used to provide a good understanding of the dynamic response of the bundle.

Dependent upon the particular tube bundle configuration, the instability was determined to be very strong, as one extreme, or, as in the case of the full bundle of finned tubes, relatively weak. In the former case the instability was considered "strong" by virtue of the loud noise associated with impacting/rattling that accompanied the instability and was readily detected by ear. In the latter case, while sensory observations allowed one to identify an increase in vibration amplitude, the amplitudes were not such that they resulted in violent impacting between tubes or within the baffle holes.

An important result of the test program was the evaluation of several field fixes, that is, corrective action that could be taken in the field on a unit with a tube vibration problem. While removal of row U tubes (Fig. 8a) proved to aggravate the problem, in the sense that the critical flowrate was decreased by 14 percent from the full tube value, stiffening of row U tubes and pass lanes in the far (Fig. 8b) and both (Fig. 8c) window regions served to increase the critical flowrate by 24, 32, and 46 percent respectively (see Table 8). However, it must be remembered that the creation of pass lanes serves to decrease the shellside flow velocity for a given flowrate and will, therefore, effect heat transfer. The reduction in heat transfer surface area by virtue of removing tubes will, of course, also reduce heat transfer. This emphasizes the need for a "systems approach" to design which includes both heat transfer and tube vibration together.

From the sensory observations documented in the Appendix, and the vibration response data, it is readily concluded that the dynamic response of a heat exchanger tube bundle is very complex and varies with tube location as well as from tube to tube within a given location. In particular the following general observations can be made:

- Impacting/rattling during instability can excite well defined higher harmonics of the instability mode frequency (see Fig. 15) or can excite a band of frequencies nominally centered at the instability mode frequency (see Fig. 19)

- In many cases the instability mode frequency shows a tendency to increase with increasing flowrate (see Fig. 15) and to decrease with decreasing flowrate (see Fig. 19)
- While theory[3] shows that coupling with adjacent tubes is not a necessary condition for fluid-damping-controlled instability, the stiffer stainless steel tube of case 9 "locks on" to the frequency of the brass tube at instability (see Fig. 15c).

The critical flowrate given in Table 8 is the lowest critical flowrate, as determined from sensory observations, for the particular tube bundle listed. As discussed above and documented in the Appendix, different groups of tubes within a given tube bundle experience instability at different flowrates and often exhibit decidedly different dynamic behavior (for example, an abrupt increase in vibration level versus a gradual increase).

Differences in behavior between the near and far window region tubes can, of course, be attributed, in part, to the differences in tube support and associated mode shapes (see Fig. 10). However, for tubes similarly supported, as in a particular window region, the differences in dynamic behavior can be attributed to variations in the flow distribution throughout the bundle and the fact that, in addition to variances in magnitude of the velocity vector (see Fig. 3), the angle of incidence with respect to the specified tube bundle layout (in these tests "30° triangular") also varies (see Figs. 2 and 3). Locations on the periphery and the bypass flow between tube bundle and shell will also result in "singularities."

A further factor, contributing to differences in dynamic behavior, is the tube-to-tube variance in intermediate support conditions (lateral loading and/or amount of clearance between tube and baffle hole). These variances, caused by lack of tube straightness, gravitational forces, and steady fluid loadings, will effect tube damping and to a lesser extent tube vibration frequencies. While such variances are expected to have a relatively minor effect on the onset of fluidelastic instability, they may be expected to have a significant effect on the subcritical response of the tubes and the response characteristics at instability. As an example of the latter, damping is known to effect the "abruptness" with which instability initiates:[12] For a heavily damped tube the instability is

typically very sharp (abrupt), while for a lightly damped tube it is often "more gradual," and, therefore, ill-defined.

ACKNOWLEDGMENTS

This work was performed under the sponsorship of the United States Department of Energy, Office of Advanced Conservation Technologies, and represents a U.S. contribution to the International Energy Agency (IEA) Program of Research and Development on Energy Conservation in Heat Transfer and Heat Exchangers. The continuing encouragement and support of Drs. W. H. Thielbahr and J. J. Eberhardt of the US/DOE are appreciated. The program is an element of the Physical Processes Project within the Energy Conversion and Utilization Technology (ECUT) Program of US/DOE.

The authors gratefully acknowledge the assistance of J.A. Jendrzejczyk and D. M. Engel in the setup and conduct of the tests and in processing of the test data; Mr. J. G. Withers of Wolverine Tube Division, UOP, Inc., for his efforts to provide the finned tubing; Dr. S. S. Chen for analysis of the coupled mode response using the computer code AMASS; and Drs. J. M. Chenoweth and J. Taborek of HTRI for consultation on the selection of test parameters, including field fixes, and the analysis and interpretation of test data.

REFERENCES

1. Wambsganss, M. W., Halle, H., and Chenoweth, J. M., "A DOE-Sponsored Program on Heat Exchanger Tube Vibration," Proc. 16th Intersociety Energy Conversion Engineering Conference, Vol. 1, pp. 595-599, ASME (1981).

2. Halle, H., and Wambsganss, M. W., "Tube Vibration in Industrial Size Test Heat Exchanger," ANL-CT-80-18, March 1980.

3. Chen, S. S., "Instability Mechanisms and Stability Criteria of a Group of Circular Cylinders Subjected to Cross-Flow; Part I: Theory," ASME Paper No. 81-DET-21 (To be published in ASME J. Mech. Des.).

4. Chen, S. S., "Instability Mechanisms and Stability Criteria of a Group of Circular Cylinders Subjected to Cross Flow; Part II: Numerical Results and Discussions," ASME Paper No. 81-DET-22 (To be published in ASME J. Mech. Des.).

5. Yeung, H. C., and Weaver, D. S., "The Effect of Approach Flow Direction on the Flow Induced Vibrations of a Triangular Tube Array," ASME Paper No. 81-DET-25 (To be published in ASME J. Mech. Des.).

6. Soper, B. M. H., "The Effect of Tube Layout on the Fluidelastic Instability of Tube Bundles in Cross Flow," ASME Symposium HTD, Vol. 9, Flow Induced Heat Exchanger Tube Vibration - 1980, editors J. M. Chenoweth and J. R. Stenner, 1980, pp. 1-9.

7. Weaver, D. S., and Grover, L. K., "Cross-Flow Induced Vibrations in a Tube Bank - Turbulent Buffeting and Fluid-Elastic Instability," J. Sound and Vibration 59(2), 277-294 (1978).

8. Shin, Y. W., Jendrzejczyk, J. A., and Wambsganss, M. W., "Vibration of a Heat Exchanger Tube with Tube/Support Impact," ASME Paper No. 77-JPGC-NE-5 (1977).

9. Chung, H. H., "Analysis Method for Calculating Vibration Characteristics of Beams with Intermediate Supports," ANL Technical Memorandum ANL-CT-79-41, July 1979.

10. Chen, S. S., "Dynamics of Heat Exchanger Tube Banks," Trans. ASME, J. Fluids Eng. 99, 462-469 (1977).

11. Chen, S. S., and Jendrzejczyk, J. A., "Experiment and Analysis of Instability of Tube Rows Subject to Liquid Crossflow," ANL-CT-81-29, September 1981.

12. Chen, S. S., and Jendrzejczyk, J. A., "Experiments on Fluid Elastic Instability in Tube Banks Subjected to Liquid Cross Flow," J. Sound and Vibration 78(3), 355-381 (1981).

APPENDIX

Summary of Sensory Observations: Cases 6-15

The tube bundle was backlighted and sensory (sight, sound, and feel) observations of tube bundle response were made as the flowrate was changed. In particular, tube motion was detected by sighting down the bores of the tubes, or by holding a finger against the tube ends where they come through the tubesheets. Rattling and impacting were audible and readily detected by ear. A case-by-case documentation of sensory observations made during testing is given below.

CASE 6

Full Bundle - 14-in. Nozzles

Flowrate (gpm)	Observation
1410	Slight quivering, including tubes A-21, V-6, W-7, W-39, W-41
1820	Quivering in tubes near shell periphery rows U, Y, G, and F
2020	Essentially unchanged
2100	More activity at"bottom" of tube rows of U through X than at top
2150	Instability and impacting in central region; most tubes in far window vibrate
	Note: During a subsequent test instability initiated at 1980 gal/min

CASE 7

Full Bundle - 10-in. Nozzles

Flowrate (gpm)	Observation
1160, 1410	Quivering of tubes A-21 and 23
1600	Quivering of additional tubes A-25 and 27, V-6 and 42, and Y-37
1800	Less quivering of A-23. A little vibration observed in row AA, tie bolt Z-14, top tubes W-9, X-10, Y-11. Tube Y-37 moderately active.
2000	Impacting in row U and some neighboring tubes.
	Note: During a subsequent test instability initiated at 1970 gal/min. Posttest observations indicated that

central region tubes U-21 through 27, and V-20 through 24 were vigorously shaken.

CASE 8

Row U Removed

Flowrate (gpm)	Observation
1400	Tube A-27, C-17, and 31, quivering felt with finger
1600	Slight vibration observed in far window near shell periphery, tubes V-6, V-42, X-38, and Y-37
1680	No impacting yet
1700	Impacting initiates, row V-16 through 30, Tubes W-37 and 39 active (not impacting)
1800	Impacting, row V-14 through 36 vibrating in lift (transverse-to-flow) direction, W-17 through 31 some vibrating at about 45° angle. Tubes X-32, 34, 36 and Y-37 active
2000	Additional impacting tubes X-22, 24, 26 (26 in lift direction). Row W tubes now vibrating in drag (parallel-to-flow) direction. Row G tubes in far window start quivering, tube C-17 quivers intensely
2200	Additional impacting, tubes V-10 and 12
3000	Impacting of some tubes in row Y
1450	With decreasing flow, approximate flowrate where instability ceased

CASE 9

Row U Stiffened

Flowrate (gpm)	Observation
1100	No significant observation
1400, 1600	Row A tubes (A-21, 23, 25, 27) experiencing low-level vibration
1680	Tube (V-6, V-8, W-7, V-42, W-41) motion can be observed
1800	Row A tubes "quieted down"
1900, 2000	No change
2200	Vibration amplitude increases for tubes V-42 and W-41; can feel vibration at tube ends
2400	No change

2450	Distinctive noise associated with tube impacting can be heard; tubes V-24, 26 experiencing large amplitude motion
2530	Tubes in center of Row V vibrating with large amplitude (V-20, 22, 24, 26); also U-25, 27; V-40, 42; and W-41. Four-span tubes (C-15, 17; B-16, 32; and C-31, 33) vibrating significantly at a "high" frequency
2620	Large amplitude vibration general in far window (3-span tube) region; all tubes in row U vibrating "strongly"

CASE 10

Pass Lane - Far Window Region

Flow Rate (gpm)	Observation
900	No significant observations
1200	No significant observations
1400	Can "feel" high frequency "hum" on tubes A-21, 23, 25, 27
	Nothing on tubes A-19, 29
	Nothing in far window
1600	Same observations as for Q = 1400
1800	High-frequency "hum" moves to tube C-15 and those in immediate vicinity
	Can "see" low-level "orbiting" of W-7 and V-6
2000	Can see low level orbiting of V-6, W-7, W-9, V-42
	Near window behavior same as 1800
2200	Same as 1800 - can see motion - difficult to "feel"
	Near window the same
	No impacting or rattling noise heard
	Tube C-17 buzzing (by "feel")
2400	Can begin to hear noise from near window
	Can begin to feel more general motion in near window - primarily high frequency
2500	Can start to hear impacting/rattling noise from far window
	Activity in near window the same as 2400
	Tube B-33 has high-frequency buzz

2600 Could consider as instability threshold although impacting would not be considered violent - far window bundle definitely "wants to go" but can't quite "do it"
A lot of motion in row U - all of the "bottom" tubes (i.e., U-27 to U-43) of row U as well as Row U, V, and W tubes near the center are experiencing large motion
However, there is little activity "at the top" of the far window region, viz., tubes in vicinity of U-5 and U-7

2700 All of tubes in rows W, V, and U are "going" ("top" now going as well as "bottom")
General large amplitude vibration in far window region
Near window tubes still vibrating at higher frequency

2800 Tubes in far window region definitely undergoing an instability; however, it's a "nonviolent" instability - the impacting/rattling noise associated with instability is not "solid" - seems to want to "come and go"

2900 Same as 2800
Instability "not violent"
A "different sound" could be heard coming from the HX - sort of a roar one would associate with flow noise

3000 Same as 2900
More motion near "top" of far window

2800 Could still hear flow noise "roar" from HX
Other observations unchanged

2600 Vibration in far window region quieted down significantly
Still large amplitude motion in rows U and V - again more motion at the "bottom" of row
Flow noise roar gone

2400 In going from 2600 to 2400 gpm impacting/rattling noise from far window region just about dropped out.
Only slight impacting noise from rows U and V tubes near the "top" of the rows (almost no motion at the "bottom" of rows U and V)

	Near window quiet (to the ear) - still can "feel" high-frequency buzz on tube C-15 and adjacent tubes
2200	Slight impact noise from far window region near the "top" - while at 2200 gpm the noise stopped. All's quiet!!
	Can still feel high-frequency buzz at tube C-15
2000	Same as 2200

CASE 11

Full Bundle - 10-in. Nozzles

Flow Rate (gpm)	Observation
1000 - 1200	Quiet - not much happening
1400 - 1600	Can begin to "see" motion of tubes W-41, V-6, V-8, W-7
1800	Tubes W-7, W-9 "nervous"
1900 - 2100	Unit relatively quiet - no rattling or impacting audible - slight motion visible at top and bottom of far window region
2140	Can start to hear impacting - large motion on tube U-23 also tube U-13 - would identify as threshold of instability
2200	Tubes in far window region rows U, V, W, and X vibrating with large amplitude - most "action" in top half of far window region - going "good," but not "violent"
2300	Intermittent in sense of already "going good" but wanting to "go better"
2400	General large amplitude vibration - primarily rows U, V, and W - does not seem as violent (noisy) as in previous full bundle test
2600	No significant change - no noticeable motion in near window region

In sweeping down from 2600 gpm -

2160	Noise starts to go intermittent - wants to "drop out"
1750	Only slight impacting (few tubes) can be heard
1700	Threshold for quietness - all signs of rattling/impacting gone

CASE 12

Pass Lanes - Near and Far Window Regions

Flow Rate (gpm)	Observation
600-1600	No significant observation - all's quiet
1800	Tubes at top of far window region showing slight "nervousness" - tubes U-7, W-7, V-6 showed most motion - no visible motion in "center" of tube row. Can feel high-frequency "buzz" on near window tubes C-17, B-16, B-18 (C-17 going the most)
2000	Same observations as for Q = 1800 gpm
2200	From shell view port can see tubes V-26 and X-26 vibrating - Can now see motion at bottom of far window - particularly tube W-41 - Observations of 1800 gpm still valid
2400	Can feel high frequency "buzz" of C-15 and C-17 (now buzzing "good"); C-29 and C-31 also felt to be buzzing but not quite as strong - From side port on shell can see V-26, X-26, and W-26 vibrating (V-26 "goes" the most, W-26 the least); corresponding tubes V-22 and X-22 not vibrating as much - Observation in far window made from tubesheet as for 1800 gpm.
2600	Tubes at top of far window (V-6, U-7, W-7) seem to have quieted down some though still whirling - Tubes at bottom of window region going as before - No audible impacting/rattling - Through side port on shell can see tube T-24 vibrate in "saddle" support
2800	Still no audible impacting/rattling noise - Through side port can see tube in outer row (AA-27) vibrating - Bottom of far window now most active - No large motion apparent in center of window region as viewed from tubesheet
2870	First heard impacting/rattling noise - Could be considered threshold flowrate for instability
3000	Impacting not violent - gives feeling it wants to "go more" but can't quite make it - Row U from center to bottom (U-27 to U-43) vibrating strongly; however, not

	upper tubes in row (U-5 to U-21) - From side port can see tube V-26 going strongly and "wanting to go more" - Motion of V-26 seemed to be synchronized with impacting/rattling noise - Tube T-24 observed to be vibrating in saddle but not tubes T-22 or T-26
3100	Rows U, V, and W now vibrating strongly from "top to bottom" - Well into instability - However, instability not "violent" - No motion observed in near window region
3200	Same observations as for 3100 gpm
3300	Instability seems to be "locked-in" a little more strongly - nothing to observe in near window
3500	Same as for 3300 gpm

Flowrate was slowly decreased from 3500 gpm -

2980	The "more-or-less" steady impacting/rattling noise, characteristic of instability, became intermittent - i.e., impacting/rattling noise comes and goes
2500	All's quiet!

CASE 13

No-tubes-in-window (NTIW)

Flow Rate (gpm)	Observation
1620 - 2600	No significant tube vibration
	Viewing through far window region port (see Fig. 6), can observe slight vibration of tubes in saddle row T (tubes T-16 to 20)
	Tie bar (AA-17 and 31) vibrating with peak-to-peak amplitude of approximately 1/16 in.
3000	No significant tube vibration
	Tie bar AA-31 vibration audible, peak-to-peak amplitude of approximately 1/8 in.
3400 - 4590	No significant tube vibration
	Amplitude of vibration of tie bar AA-31 increased to approximately 1/4 in. peak-to-peak

CASE 14

NTIW - Finned Tubes

Flow Rate (gpm)	Observation
1000	No observable vibration - all's quiet
1500 - 2000	Tie bars in far window region vibrating slightly
2500 - 3500	Can "feel" vibration of many tubes - others "feel dead" Tie bar vibration levels increasing - can hear tie bar in near window region impact against shell wall
4000 - 4500	General low level vibration of essentially all tubes can be felt Vibration "feels" greater at inlet side Can see tubes vibrate in baffle holes
5000 - 6000	No significant change Full bundle experiencing low level vibration

CASE 15

Full Bundle - Finned Tubes

Flow Rate (gpm)	Observation
600 - 800	No observable vibration
1000 - 1400	Can feel low level vibration in row A tubes
1600	Low level vibration barely discernible in rows U and V (tubes 20 to 30)
1800	Tubes at inlet still vibrating at low levels Tubes Y-37, X-38, W-41 (all peripheral tubes) have increased in vibration level
2000	Tubes at inlet seem to have "quieted down" The same tubes noted to be vibrating at Q = 1800 gpm are still vibrating noticeably
2200 - 3000	Additional tubes (V-40, V-42, and U-43) are vibrating - amplitudes are moderate - no audible impacting/rattling Can "feel" activity in near window at nozzle inlet
3200	Can hear rattling/impacting noise from bottom of near window region Tube motion at bottom of far window region has increased
3400	Tube motion at top of window regions with tube motion greater in far window - No observable tube motion in

	center of row U as would be expected from previous tests
3500	No significant change Tubes at bottom of near window region vibrating the most
3600	Impacting noise level from near window tubes has increased
3900	No change - still no detectable motion in middle of row U
4100	Can observe motion in all of row U
4200	Row V now vibrating - also, tubes at top and bottom of both window regions are vibrating
4400	No change - impacting noise did not increase with vibration of rows U and V tubes

Distribution for ANL-CT-81-42

Internal:

R. S. Zeno
G. S. Rosenberg
M. W. Wambsganss (50)
R. E. Holtz
A. R. Evans
S. S. Chen
H. H. Chung
H. Halle (90)
J. A. Jendrzejczyk
W. P. Lawrence
T. M. Mulcahy
M. Weber
ANL Patent Dept.
ANL Contract File
ANL Libraries (3)
TIS Files (6)

External:

DOE-TIC, for distribution per UC-95f (246)
Manager, Chicago Operations Office, DOE
Director, Technology Management Div., DOE-CH
E. Gallagher, DOE-CH
President, Argonne Universities Association
Components Technology Division Review Committee:
A. Bishop, U. Pittsburgh
F. W. Buckman, Consumers Power Co.
R. A. Greenkorn, Purdue U.
W. M. Jacobi, Westinghouse Electric Corp., Pittsburgh
M. A. Schultz, North Palm Beach, Fla.
E. E. Ungar, Bolt, Beranek and Newman, Inc., Cambridge, Mass.
J. Weisman, U. Cincinnati